ADVANCED MATERIALS
www.advmat.de

Shape Memory Alloy (SMA) Actuators: The Role of Material, Form, and Scaling Effects

Min-Soo Kim, Jae-Kyung Heo, Hugo Rodrigue, Hyun-Taek Lee, Salvador Pané, Min-Woo Han,* and Sung-Hoon Ahn**

Shape memory alloys (SMAs) are smart materials that are widely used to create intelligent devices because of their high energy density, actuation strain, and biocompatibility characteristics. Given their unique properties, SMAs are found to have significant potential for implementation in many emerging applications in mobile robots, robotic hands, wearable devices, aerospace/automotive components, and biomedical devices. Here, the state–of–the–art of thermal and magnetic SMA actuators in terms of their constituent materials, form, and scaling effects are summarized, including their surface treatments and functionalities. The motion performance of various SMA architectures (wires, springs, smart soft composites, and knitted/woven actuators) is also analyzed. Based on the assessment, current challenges of SMAs that need to be addressed for their practical application are emphasized. Finally, how to advance SMAs by synergistically considering the effects of material, form, and scale is suggested.

1. Introduction

Shape memory alloys (SMAs) are a class of materials that, after being deformed at a lower temperature, can recover their shape when heated above a certain temperature. Because of this ability, SMAs have been considered as alternative actuating building blocks for replacing conventional actuators, such as electric and fuel-powered motors. In addition, given their high work density, they enable reductions in weight and size while being able to produce complex motions and have highly tailored behaviors. For these reasons, SMAs have been employed as components in wearable devices, mobile robots, robotic end-effectors, automotive/aerospace components, and biomedical devices.

In 1932, Ölander discovered the shape memory effect (SME) in an alloy of Au and Cd.[1] The SME enables recovery from plastic deformation (toward the initial shape) by exploiting changes in the crystalline structures of martensite and austenite. Chang and Read showed that SMAs generated mechanical work (cyclic lifting).[2] In 1961, the US Naval Ordnance developed alloys of nickel and titanium (Ni–Ti, nitinols) that were less expensive than earlier SMAs, easier to use, and enhanced biocompatibility characteristics.[3,4] Early commercial products (in the 1970s) used SMAs to trigger 1D shape changes in pipe couplings and electrical connectors.[5] The thermal hysteresis and cyclic deformation performance of SMAs were then investigated to expand the application of SMA actuators to many devices.[3,6,7] Spring-type SMA actuators were developed to enhance actuation-mediated deformation. In 1988, nitinol wires were embedded in a laminated polymer matrix composite.[8] These actuators produce continuous, multidimensional, and complex motions. Today, SMA actuators are applied in

M.-S. Kim, S. Pané
Institute of Robotics and Intelligent Systems
ETH Zurich
Zurich CH-8092, Switzerland
E-mail: vidalp@ethz.ch

J.-K. Heo, S.-H. Ahn
Department of Mechanical Engineering
Seoul National University
Seoul 08826, Republic of Korea
E-mail: ahnsh@snu.ac.kr

H. Rodrigue
School of Mechanical Engineering
Sungkyunkwan University
Gyeonggido 16419, Republic of Korea

H.-T. Lee
Department of Mechanical Engineering
Inha University
Incheon 22212, Republic of Korea

M.-W. Han
Department of Mechanical, Robotics and Energy Engineering
Dongguk University
Seoul 04620, Republic of Korea
E-mail: mwhan@dongguk.edu

S.-H. Ahn
Institute of Advanced Machines and Design
Seoul National University
Seoul 08826, Republic of Korea

The ORCID identification number(s) for the author(s) of this article can be found under https://doi.org/10.1002/adma.202208517

DOI: 10.1002/adma.202208517

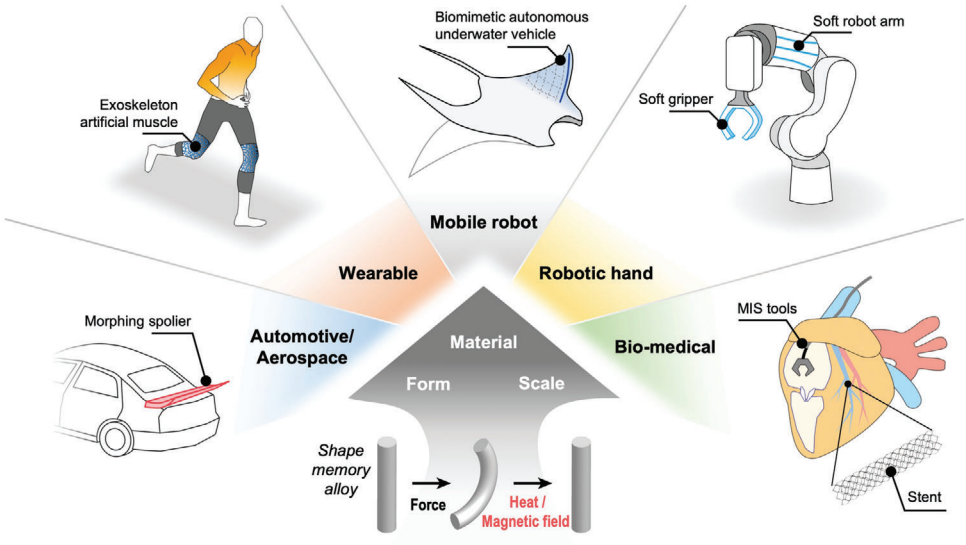

Figure 1. Depending on the material, form, and scale, SMA-based actuators find a wide range of applications in wearable devices, mobile robots, robotic hands, automotive/aerospace appliances, and biomedical devices.

microelectromechanical systems (MEMS), the biomedical field, and devices for space applications.[9–18]

Over the last two decades, applications of SMA actuators have expanded to include robotic hands and wearable devices; precise actuation, manufacturing technology, mechanical design, and range of available SMA materials have greatly improved. Through recent advances (in the 2010s) in SMA materials and fabrication technology, small-scale actuators with complex designs have been developed.[19–36] The wide range of technologies available today allows SMA systems to be tailored in terms of material, form, and scale, to specific applications.

Here, we discuss recent SMA actuator developments in terms of material, form, and scale (**Figure 1**). We first look at existing SMA materials and compare the characteristics of thermal SMAs (TSMAs) and magnetic SMAs (MSMAs) using actuation performance indices and look at the different surface treatments used to modify their properties. Next, we look at the form of these materials, and how it is selected for achieving a specific deformation, how complex motions are produced, and ultimately how to leverage these characteristics to fabricate freestanding actuators, composites, or textile composites. The following section looks at the actuator scale and how this factor significantly affects actuation speed and complexity. Finally, the advantages and limitations of SMA actuators are described, and we suggest how to synergize SMA material, form, and scale for further improvement of SMA-based structures.

2. Results

2.1. Material

SMAs operate via a crystalline transformation triggered by different inputs. SMA materials are broadly categorized according to their base material or input source. Two types of SMAs are distinguished based on their input source: TSMAs and MSMAs. An overview of the materials used to fabricate SMA-based actuators is shown in **Figure 2**a, including the working temperatures, input sources, and operating temperature range of commercialized products. These features serve as a guide for selecting a SMA for a given application.

More information about the performance of SMAs and other smart materials is available in Tables S1 and S2 (Supporting Information). Additionally, the National Aeronautics and Space Administration (NASA) database includes tools for shape memory (SM) materials that provide further information based on a comprehensive literature survey.[37] Similar to an Ashby chart,[38] SM material properties can be compared based on performance indices. For example, in the actuator design step, an appropriate SMA is selected based on a scatter chart of strain as a function of its austenite temperature. Databases can be combined with machine learning.[39]

2.1.1. Thermal Shape Memory Alloys

TSMAs (discovered in the 1930s) have become the most widely used type of SMAs. As the name indicates, the crystalline phase of a TSMA depends on temperature. A deformation cycle begins when the twinned martensite phase is converted into detwinned martensite through application of an external stress. This martensite phase (twinned or detwinned) begins to change to the austenite phase when the temperature is increased above the austenite start temperature (A_s), and becomes fully austenite when the austenite finish temperature (A_f) is reached (Figure 2b).[40] The reverse transformation is accomplished by cooling the SMA to the martensite start temperature (M_s); phase reversal is complete at the martensite finish temperature (M_f). The main TSMA performance indices are the transformation temperatures; A_f serves as the representative temperature in Figure 2a because this is the temperature that must be reached in an actuation cycle. However, SMAs can generally handle higher temperatures. Figure 2a shows the transformation temperature

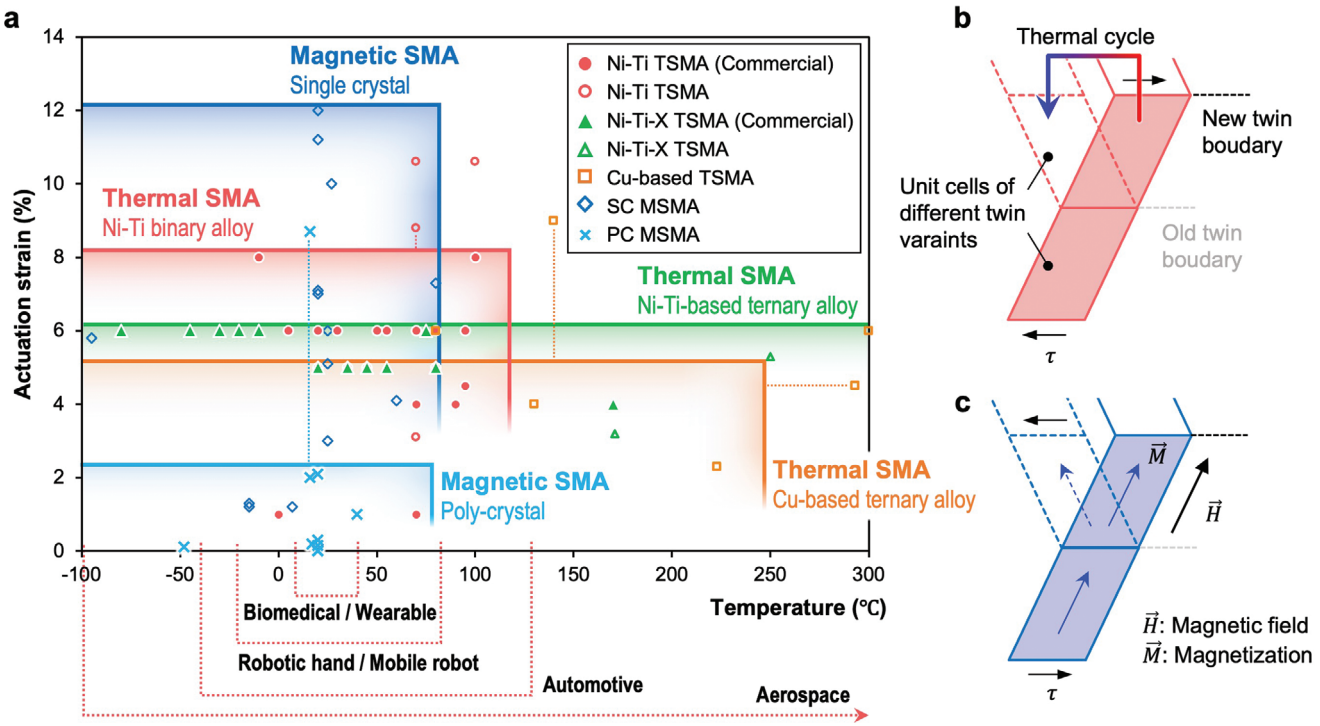

Figure 2. a) Comparison of different SMA materials in terms of actuation strain and temperature. The temperature refers to the A_f transformation temperature for thermal SMAs (TSMAs) and working temperature for magnetic SMAs (MSMAs). The shape memory mechanisms of b) TSMAs and c) MSMAs.[40]

and actuation strain of different TSMAs. There are three representative groups: Ni–Ti binary alloys, Ni–Ti-based ternary alloys, and Cu-based alloys. Of these, Ni–Ti-based alloys are the most widely commercialized.

Compared to Cu-based alloys, Ni–Ti-based SMAs (also known as nitinols) show higher actuation strains, larger generated forces, higher corrosion resistance, and enhanced biocompatibility characteristics.[40] Their transformation temperatures range from −150 to 100 °C and can be tuned by adjusting the nickel concentration.[41] The recoverable strain is higher than that of other TSMAs. Their biocompatibility characteristics make such alloys optimal for biomedical applications. As their transformation temperatures are low, ternary alloys of NiTi with other elements have been developed by adding Pd, Zr, Pt, and Au, yielding high-temperature SMAs that find applications in the automotive and spacecraft fields. The higher transformation temperatures allow these SMAs to cool rapidly at room temperature.

By contrast, Cu-based SMAs exhibit less temperature hysteresis, better machinability, and lower cost than nitinol. The transformation temperature can be adjusted from −200 to 200 °C by changing the alloy composition.[40] However, given their poor recovery strain and corrosion resistance, Cu-based SMAs have seen fewer commercialization attempts. Other alloys include Au–Cd, In–Tl, Au–Cu, Fe–Pd, and Fe–Pt alloys, but these often exhibit both poor recovery strain and corrosion resistance and are expensive.[42–45]

In general, the performance of TSMAs is determined by the composition of elements and their crystallization. The transformation temperature of nitinol can be adjusted by modifying the concentration of nickel. For example, as the nickel concentration increases from 50% to 51%, the transformation temperature decreases linearly from 92 to −46 °C with a slope of 83 °C (at% Ni)$^{-1}$ at lower Ni concentrations and nonlinearly at higher concentrations.[41] Doping with a third element (i.e., Fe, Co, Cu, Al, V, Cr, Mn, Zr, Hf, Pd, Pt, and Au) leads to a monoclinic martensite phase after the martensitic transformation which increases the martensitic temperature and results in a larger temperature hysteresis.[46] The actuation strain, caused by the martensitic strain, varies by the pathways of martensitic transformations, from austenite to martensite (i.e., B19′, B19, and R). For example, nitinol monoclinic B19′ yields the maximum strain, followed by orthorhombic (B19) with the least transformation strain seen in the trigonal (Rhombohedral-R) phase.[47] The crystallization also affects the actuation strain; single crystalline SMAs have usually a higher strain than polycrystalline due to the presence of grain boundaries, defects, precipitates, etc. Actuation stress also depends on the critical stress, which is determined by the nucleation of the crystal.[48] The actuation speed is related to the heating and cooling speed as TSMAs are actuated by temperature changes. The rates of heating and cooling depend on the heat transfer mechanism and, therefore, slow speed due to limitations in cooling is regarded as a limitation of TSMAs.

TSMAs are usually fabricated from ingots, powder metallurgy, physical vapor deposition, among others. Ingots are produced by common commercial melting methods, such as vacuum-induction melting and vacuum-arc melting. Then, the ingot is processed by cold drawing and annealing to make a 1D (wire) or 2D (plane) structures. These structures are processed to a product

with complex shape and adequate surface properties by machining, laser cutting, electropolishing, joining processes.[49–51]

TSMAs have a long history of commercialization and have found many practical applications, given the wide range of transformation temperatures, reliable actuation performance, and reasonable price. The most commonly used TSMA shapes are wires and plates; wires can be coiled into springs and plates can be shaped through laser cutting. However, TSMAs are not very energy-efficient because they require heat for actuation, which is associated with low bandwidths and slow actuation speeds at larger scales.

2.1.2. Magnetic Shape Memory Alloys

Magnetic fields can also be used to induce SMA phase transformations; these SMAs are termed MSMAs (Figure 2c). After Ullakko (1996) discovered the phenomenon in Fe–Ni alloys, researchers have sought to increase the recoverable strain and working temperature range.[52] Figure 2a summarizes MSMA actuation strains and working temperatures. As phase transformation can be induced either magnetically or via a change in temperature, the working temperature in Figure 2a should be maintained below the A_s in order for the magnetic field to be able to induce the phase transition. A MSMA should be kept below this temperature to allow magnetically induced phase transformation. Ni–Mn–Ga is the most widely used MSMA; Ni–Mn–Al, Fe–Pd, and Fe–Pt alloys are also commonly employed.

Similar to TSMAs, the actuation performance of MSMAs is determined by material composition and crystallization. The working temperature is generally restricted to <100 °C (due to the need to keep them below their martensitic transformation temperature).[53,54] However, the martensitic transformation temperature is varied by the Ni, Mn, and Ga composition, which changes the valence electron per atom.[55] For example, as the Ga concentration increases from 18% to 26%, the martensitic temperature changes from 176.85 to 6.85 °C.[56] Doping of Cu also increases the transformation temperature.[57,58] Meta MSMAs (Ni–Mn–X (X = Sn, In, Sb)) have emerged as one of the alternative ways to improve the material properties as they are less toxic and operate within a high temperature range.[59]

The actuation strain of MSMAs is determined as magnetic-field-induced strain (MFIS), which is varied by the strain of the twin during shear deformation. The MFIS can be enhanced by training, which reduces the resistance of the twin motion. While single crystalline exhibits 1–10% of MFIS, polycrystalline has <0.01%. Since the grain boundary suppresses the twin boundary motion that mainly affects the MFIS, polycrystalline MSMAs usually show very little MFIS.[60] In single crystal MSMAs, the MFIS can be improved by tuning the microstructures. For example, the structure of Ni–Mn–Ga, such as the five-layer modulated martensite (5 M, pseudotetragonal), seven-layer modulated martensite (7 M, pseudo-orthorhombic), and nonmodulated martensite (NM, tetragonal), determines the lattice parameter and coordinate system which increases the MFIS (theoretically 7% at 5 M, 11% at 7 M, and 12% at NM).[61] Single crystal MSMAs exhibit outstanding MFIS, but manufacturing and processing are difficult and impractical outside of research laboratories. By contrast, polycrystalline MSMAs are easier to fabricate but exhibit near-zero actuation strain due to the constraint imposed by grain boundary. Thus, to improve actuation strain, coarse-grained (highly textured) polycrystalline MSMAs were developed. The constraints were reduced by directional solidification and annealing, which increased the actuation strain.[60–62] Foaming makes high level of porosity, which has smaller pore than grain size, decreases the effect of grain boundary, and increases MFIS by 2–8.7%.[63]

The actuation response of MSMAs is in the order of 1–10 ms since applying a magnetic field immediately induces phase transformation. Compared to TSMAs which take about tens of milliseconds or more for heating only, MSMAs can generate quick motion. Also, MSMAs are more energy efficient than TSMAs as they do not use thermal energy. The work output is comparable to that of TSMAs.[64] Another significant performance index for comparing MSMAs is the magnetic field required for martensitic transformation. Usually, materials with higher MFIS require a stronger magnetic field. Thus, this trade-off between the actuation strain and required magnetic fields should be carefully considered to select an appropriate MSMA for a given application.

These MSMAs are usually prepared by melting and casting. Single crystalline MSMAs are usually fabricated using Czochralski (pulling method) and Bridgman methods.[59] Polycrystalline MSMAs are processed by melting and casting or solid-state sintering. Microwires are made by melt spinning or the Taylor drawing method. Foam structures are manufactured by the casting replication method, which consists of the liquid metal infiltration of a preform with ceramic space-holder powder acting as pore former.[63] The shape can be further formed by plastic deformation.

However, MSMAs remain under development,[65–67] and commercialized products are not widely available. Depending on the requirements of the application, the MSMAs should be further developed to obtain a wider working temperature, to increase the strain in the polycrystalline structure, and to reduce the required magnetic field for actuation. Electromagnets are commonly used to operate MSMAs, and applications in the fields of aerospace, automotives, or mobile robots can equip electromagnets with high magnetic fields (≈1 T) as they have sufficient space. On the other hand, biomedical devices have a limitation in the magnitude of the magnetic field as electromagnets with lower magnetic fields (<100 mT) are used for remote operation. Remote control has a lower energy efficiency than actuation by using on-board electromagnets.

Finding new ferromagnetic materials for MSMAs is also an important research direction for their further development and adoption. As with the invention of nitinol for TSMAs, improved materials with better chemical resistivity, better biocompatibility, and lower production costs should lead to new applications of MSMAs and bolster their commercialization.[59,68]

2.1.3. Surface Treatment on Shape Memory Alloys

Surface treatment is one of the techniques to impart special characteristics to the structure, enhancing the performance and the functions of the device. Surface treatments for SMAs include coating, physical or chemical treatment, and engraving. They can facilitate the integration of new properties and functionalities to

overcome technical challenges in existing SMAs, such as heat dissipation, light absorption, corrosion resistance, biocompatibility, and adhesion.

One of the challenges in TSMAs is their slow response time. Joule heating is widely used for actuation, which can reduce the heating time by increasing the current. However, long cooling times are a significant issue. Because of their slow thermal exchange, TSMAs display slow cooling rates, which limit the actuation speed. To overcome this, Oh et al. enlarged the surface area of a SMA spring by growing copper nanowires on the surface of the spring.[69] The nanowire forest increased the surface area 15-fold and boosted thermal convection; the actuation speed was increased to 170% that of an untreated coil. Immersion of a SMA in liquid increases the cooling speed but is impractical. A nitinol actuator encapsulated in a self-cooling hydrogel matrix maintained the required surface temperature of the SMA and ensured biocompatibility.[70]

Another challenge comes from the limited power source. Joule heating both needs an electrode (hindering the actuator design) and requires a high-capacity battery (impeding the miniaturization of mobile robots). Fuel is a prominent alternative to electric power sources. Pt enables catalytic methanol combustion (producing heat and inducing the transition). Thus, Pt-coated SMA wires can also be heated using methanol. Vaporized methanol can flow in open and closed channels; this approach has been used, for example, to induce crawling in a millimeter-long beetle robot.[71]

Lasers are commonly used for SMA actuation, but a low absorption rate in certain wavelengths limits the light source. SMAs exhibit high absorbance in the ultraviolet (UV) spectrum and low absorbance in the infrared (IR) spectrum. To expand the light sources, Kim et al. adjusted the SMA absorbance by engraving conical holes at sub-micrometer intervals, inducing a plasmonic effect that increased IR absorbance by 90%. The pattern density affected the peak absorption wavelength.[21] Also, Zaidi et al. used a metal–insulator–metal (MIM) nanostructure to change the optical properties. The MIM structure tunes light absorption to wavelengths of 532, 660, 785, and 980 nm by changing the thickness of the insulator; different light sources allow for selective actuation.[72] Such treatments can be very useful; no-contact methods (such as lasers) can then be applied for selective actuation of a SMA structure.

Nitinol itself is biocompatible but may lose biocompatibility due to corrosion. This is because corrosion causes nitinol to release Ni^{2+} ions. These ions are toxic, carcinogen, and have immune-sensitizing effects. A TiN coating can prevent this corrosion which leads to better biocompatibility and adhesion to cells.[73]

In MSMAs, the surface machining methods can reduce stress for twinning, which would lower the magnetic field required for actuation. Through nanoindentation, while the electropolished surface demonstrates elastic loading and significant pop-in of the indenter, the mechanically polished surface showed little or no pop-in. This indicates that the different surface layers make the twinning stress higher for the electropolished crystal than for the mechanically polished crystal. When the thickness of the structure gets smaller, this surface effect can be significant. Thus, the mechanically polished surface could promote the initiation of deformation and twinning in small-scale Ni–Mn–Ga actuators.[74]

As discussed above, surface treatments have empowered novel and interesting performance of SMAs to overcome technical limitations. The above examples only showed the great potential of surface treatments for improving SMA actuators, and we believe there is great potential to expand their applications of the SMAs in various fields through the development of new surface treatments and their implementation in a wider range of applications.

2.2. Form

SMAs can take diverse forms including wires, springs, composites, woven and knitted structures. Each form can be achieved by using a different manufacturing process. This section describes how actuator forms can be harnessed to expand the actuation mode from simple linear motions to bending, rotation, and torsion motions, and combinations thereof.

2.2.1. Wire and Spring

Figure 3 shows how diverse actuator forms generate various motions. Wire-type SMAs produce linear motions via longitudinal contraction. This is the simplest form for a SMA actuator; using a typical TSMA, the linear actuation strain is 3–4% and the actuation stress is 100–700 MPa.[78] A SMA wire having a mechanical structure with a rotational axis of deformation allows for joint-like rotations.

Linear springs derived from SMA wires can be used to enhance the actuator deformation length at the expense of the actuation force.[79,80] Also, torsionally prestrained SMA springs can be used to produce torsional motions.[76,81] Like SMA wires, SMA springs generate both linear and rotational motions. It is also possible to use parallel SMA elements to increase the force produced. Furthermore, combinations of linear torsional springs can be used to produce complex motions.

However, a single SMA wire or spring affording one-way motion allows for only one-way actuation. For two-way actuation, a bias element (such as a spring) should be used. Two-way-trained SMA elements produce returning forces that can serve as bias elements. However, the return motion force of bias springs is not controllable, and two-way-trained SMA elements produce less force than one-way elements. Therefore, antagonistic SMA elements are generally used for two-way actuation.

2.2.2. Smart Soft Composite (SSC) Actuators

SSCs are combinations of SMAs with low-stiffness polymeric matrices that exploit the in-plane linear deformation of a SMA to produce out-of-plane deformations of the entire structure.[82–84] For example, if a SMA wire is offset from the neutral axis of a beam made of a soft polymer, the composite can bend (**Figure 4**a).[85] In addition, scaffolds can be placed within the matrix and the orientation of the scaffold affects the bending behavior of the SSC (Figure 4b). The scaffold can be constructed of multiple layers, and motions such as symmetric, antisymmetric, asymmetric, and torsional are generated by combining various ply combinations within these layers. Similar

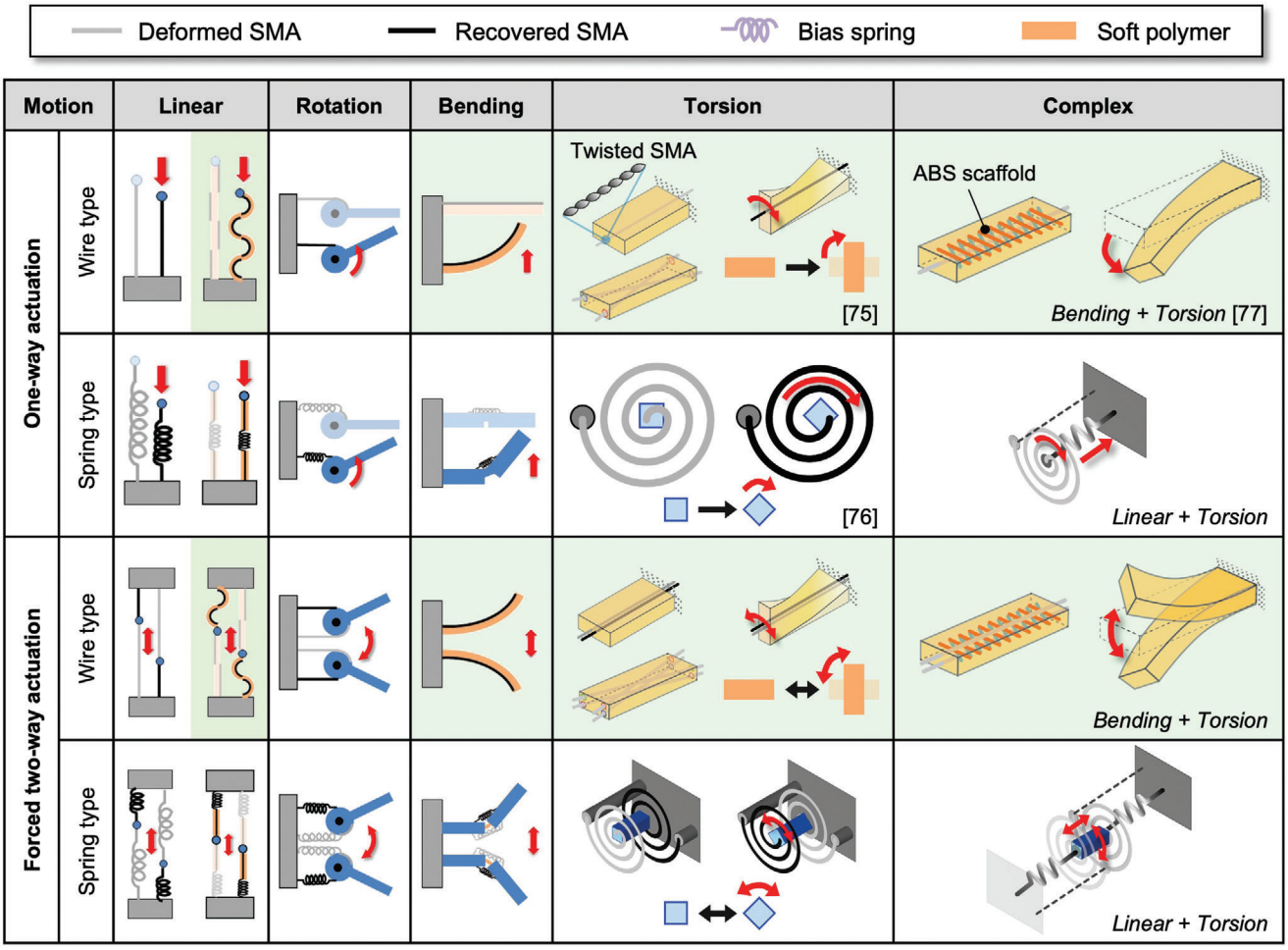

Figure 3. Diverse actuation modes generated by SMA actuators of different forms. The one-way and forced two-way actuation modes are compared among different forms of SMAs. Combinations of actuators generate complex and continuous motions. Smart soft composite (SSC) actuators are highlighted in green.[75–77]

to the principle of fiber orientation in fiber-reinforced composites, the characteristic of the scaffold varies according to their orientation, and it is possible to design scaffolds with angles ranging from −90° to 90°. In addition, the effects of the multilayer structure of these scaffolds on the properties of the actuator could be anticipated using the classical laminate theory.[86] The following are examples of representative scaffold combinations (Figure 4c–e); symmetric ply combination: [30/45/30], [45/60/45], and [75/90/75]; antisymmetric ply combination: [30/90/−30], [45/90/−45], and [75/90/−75]; asymmetric ply combination: [90/60/30] and [75/60/30].[87]

A SSC can be used to produce linear motions by assembling segments that bend in opposite directions (highlighted in Figure 3). When several such actuators are connected crosswise, the end tip of the actuator acts linearly. It is possible to produce SSC torsional motions via various means. SMA wires placed diagonally in a soft polymer enable a SSC to produce torsional deformations using the linear SMA prestrain.[88] Torsionally prestrained (twisted) SMA wires can also deliver torsional deformations via recovery of the prestrain.[75] SSCs with matrices exhibiting asymmetrical properties (after the addition of anisotropic matrix elements such as 3D-printed scaffolds) allow for torsional deformations.[77] These methods can be modified to produce both bending and torsional deformations.[89] The main advantage of SSC actuators is the ability to generate continuous and complex deformations; the principal disadvantage is the potential delamination between the soft polymeric matrix and the high-stress SMA element under cyclical loadings.

To use the SSC as a soft actuator, it is necessary to choose a matrix material whose elastic limit is not exceeded by the stress caused by the SMA phase change behavior. For stable deformation to occur, it is crucial to consider not only the material of the matrix, but also design factors such as the aspect ratio. If the material and geometry of the matrix are taken into account during design, it is feasible to achieve continuous and diverse movements, such as bending and torsion, while preventing tearing and buckling.

2.2.3. Soft Morphing Textiles

Textiles are made of fibers and can form 2D or 3D structures depending on the thread arrangement and its combination (**Figure 5**). The threads used to make textiles are single strands of

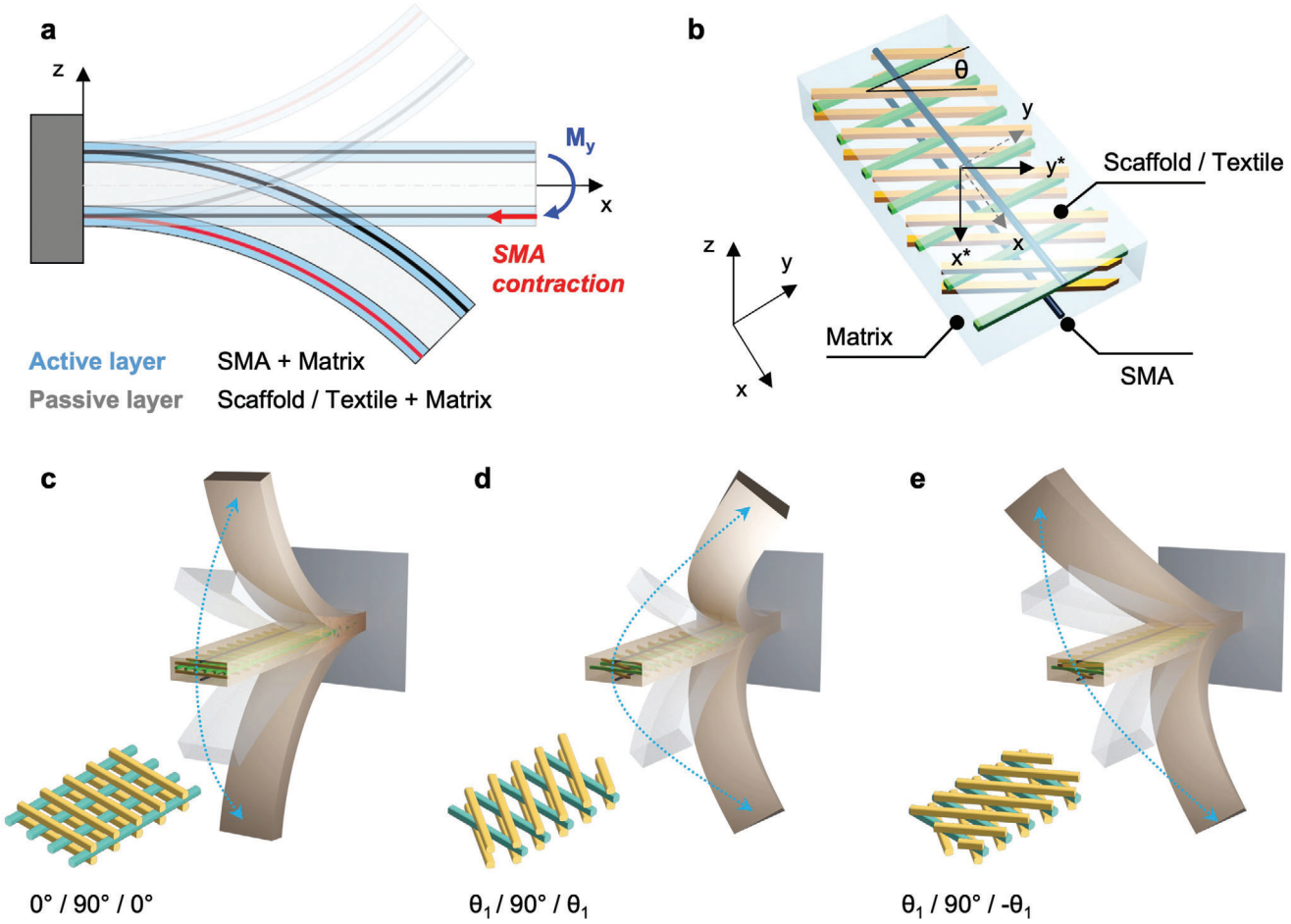

Figure 4. Schematic diagram of shape-morphing generation of SSC actuators. a) The contraction of the SMA generates a moment and a bending motion. b) Design of the SSC actuator. Asymmetric scaffold or textile layers, which have raster angle (θ), adjust the orientation of the principal axis. Bending moments can be transferred to a combination of bending and torsional motions to generate complex deformations. Symmetric or asymmetric layer combination for c) bending, d) symmetric bending–torsion, and e) antisymmetric bending–torsion. These design approaches can also be utilized for textile actuators.

wire or bundled and twisted fibers. Threads in the form of continuous strings yield flexible textiles; the flexibility, dimensional stability, and elastic recovery vary by thread arrangement. Furthermore, textiles made via continuous threading can be classified as interlaced (woven), interlooped (knitted), or intertwisted (braided) textiles depending on the thread entanglement.[93,94] Textile SMA actuators implement bending, torsion, and complex motions without the risk of delamination (unlike SSC actuators).

Wire-type SMAs can be used as substitutes for textile threads or combined with regular threads. Such textiles exploit the effects of strain generation arising from SMA phase transformations and the properties of the textiles. The direction of the force generated by the textile and the deformation limits vary according to the arrangement and combination of fibers. When the proportions of specific patterns and intertwined SMA structures that constitute the textile platform are varied, the desired modes of actuation can be achieved.

Textile composites are similar to SSCs but use a textile layer instead of the scaffold used in a SSC; its structure and deformation mechanism are similar to those of SSCs. Thus, they are usually called as woven-type SSC actuators. The behavior of these composite structures depends on the physical properties of the matrix in which the SMA is embedded. In order to increase the bending strength and modulus of composites, SMAs are incorporated between epoxy-based glass fiber reinforced plastic (GFRP) matrixes (bending modulus: 7.4 GPa). In this case, the amount of deformation is minor (between 5° and 15°), but the mechanical properties are outstanding, allowing it to be used in structures that must withstand heavy loads.[28] When applied to a polydimethylsiloxane (PDMS, Young's modulus: 1.8 MPa)-based GFRP matrix, however, considerable deformations (end-edge deformation of 200° or more) are possible. It can also resist dynamic loads (working at a wind speed of 20 m s^{-1}).[19,90,91]

Textile actuators without the polymer matrix have freestanding textile forms, providing more flexibility to the actuator and a higher degree of freedom in shape design. Interlaced (woven) textiles are created by crossing two or more sets of threads at right angles (transverse [weft] and longitudinal [warp] fibers). In such textiles, the threads are interlaced at right angles; elasticity is low but robustness and stability are maintained. The

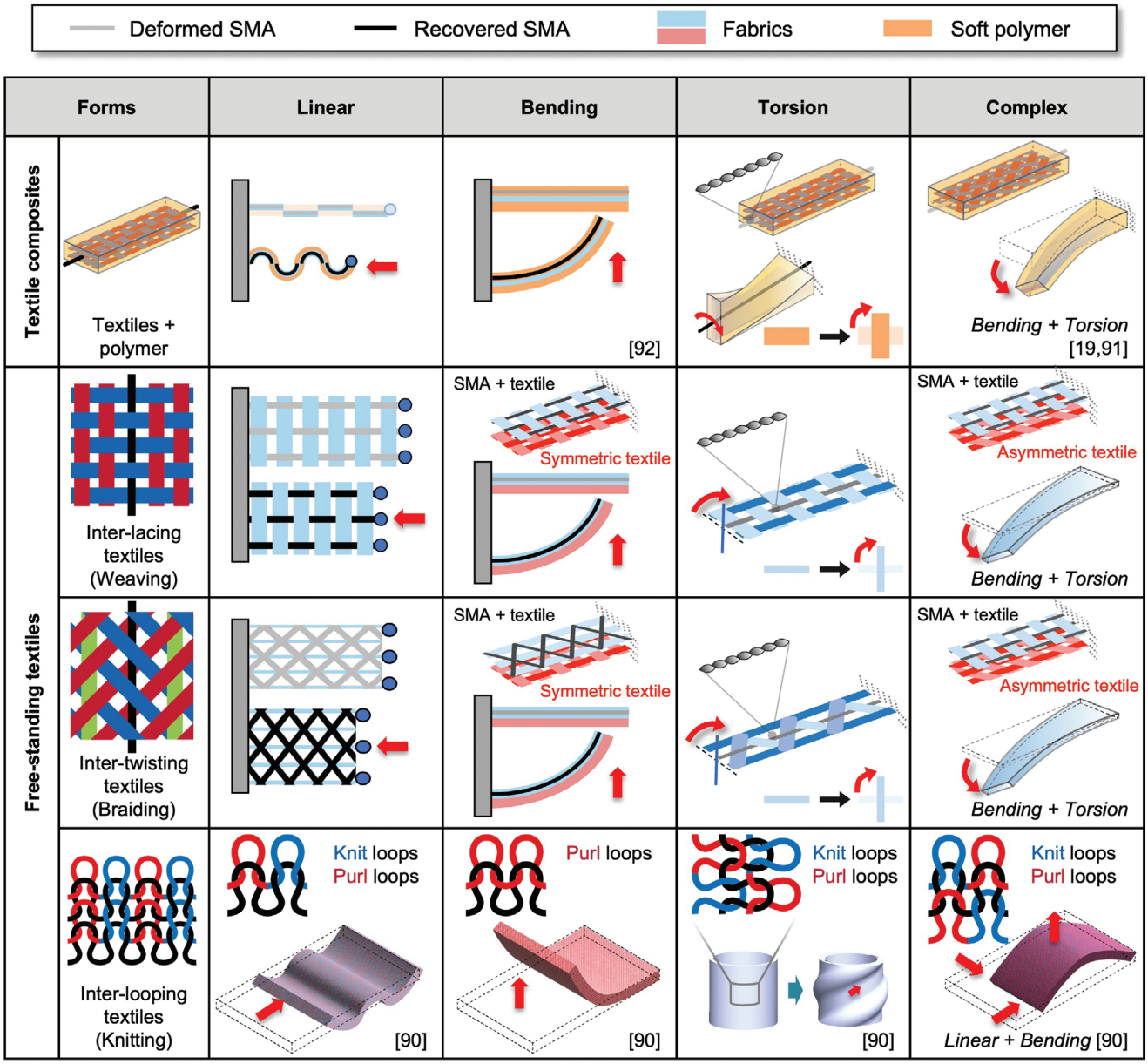

Figure 5. Actuation modes of SMA textile actuators (textile composites and freestanding textiles).[19,90–92]

mechanical properties vary by the crossing method, including the thread thickness, warp:weft ratio, "floating" proportion (weave skipping); and thread count (numbers of warp and weft yarns per unit area). The SMA is vertically arranged on the woven textile, enabling linear contraction. In a multilayer woven textile, both normal and/or asymmetrical bending motions can be induced, given the eccentricity of deformation of any particular layer. In addition, by separating the layers of woven fabric and SMA wires and by varying the angles between them, it is possible to generate complex motions (such as combined bending and torsional deformations). It is also possible to induce torsional motion by using torsionally prestrained SMA wires during weaving.[19,27,90,91]

Textiles can also be manufactured by braiding the yarn. Braiding involves intertwisted threads in the longitudinal and diagonal directions. Braided textiles are flexible and highly extensible.[95] It is possible to implement contraction and torsion by selectively actuating the SMA elements constituting the braided textile, and to implement bending by adding an additional layer eccentric with respect to the braid.

Interlooped (knitted) textiles have looping architectures; loops are connected by one or more sets of threads. Loops are porous, i.e., contain empty spaces. Thus, elasticity and wrinkle resistance are high. The two basic knitting loops vary according to the placement of the looping legs relative to the adjacent loops, yielding knit and purl loops (**Figure 6**a). These textiles have continuous

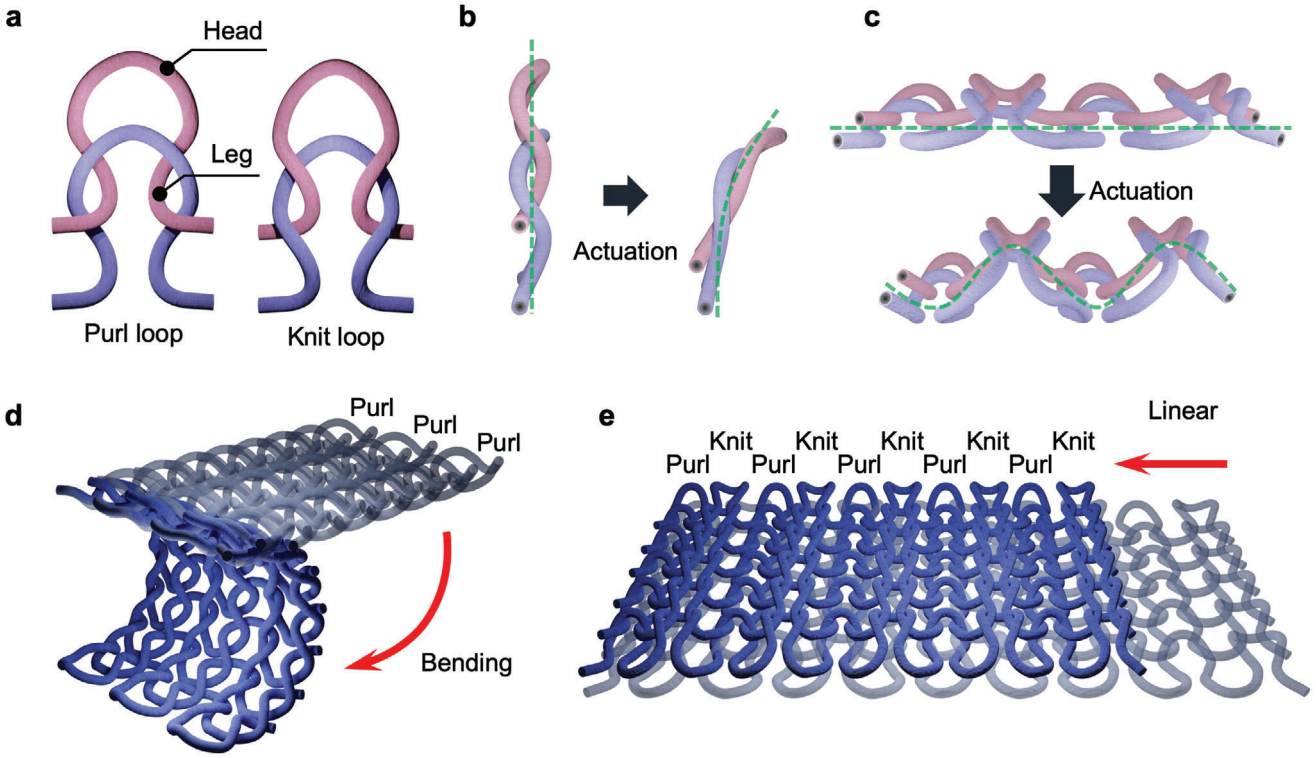

Figure 6. Schematic diagram of interlooped textile actuators. a) Unit purl and knit loop. b) Unit bending motion of a purl loop. c) Unit linear motion of two purl–knit loops. d) Bending motion of the textile. e) Linear motion of the textile.

loops; each loop is physically constrained by the other loops in contact in the transverse direction (course) and longitudinal direction (wale). A textile with a single loop pattern exhibits bending motion (i.e., the textile curls in one direction); the extent of bending can be adjusted by varying the thicknesses of the thread and size of the loop (Figure 5, details in Figure 6b,d). Loop curling occurs in both the up–down and left–right directions centered on the loop; linear motion of the textile actuator can be induced by arranging the loop-rolled structures in opposite directions (Figure 5, details in Figure 6c,e). Alternating knit and purl loops generate diagonal torsional forces, triggering asymmetrical bending. If a cylindrical geometry is employed and actuated, a torsional mode is generated along the outer surface of the cylinder (Figure 5).[92]

2.2.4. From Forms to Actuators

The implementation of the forms allows the actuators to improve their performance. It can amplify the deformation ratio or demonstrate complex shape morphing. Also, the actuation force can be changed in terms of direction or type (i.e., point load, distributed load) for specific applications. It can exhibit other interesting performances, such as extreme compliance, shape retention, and high strength structure.

Figure 7a compares the actuation stress and deformation ratio for the different forms. To compare various actuators, the values are normalized. As the wire is the primary energy source and the force is proportional to its cross-section area, the actuation force is converted into the normalized actuation stress by using Equation (1)

$$\sigma = \frac{F}{nA_{\mathrm{SMA}}} \tag{1}$$

where σ, F, n, and A_{SMA} represent the normalized actuation stress, the actuation force of the actuator, the number of wires, and the cross-sectional area of the SMA wire, respectively. Tip force represents the actuation force of the bending actuator. To compare the deformation ratio in the same way (i.e., length), vertical tip deflection is assumed as a deformation of the bending actuator (Figure S1, Supporting Information). As a result, overall, there is a trade-off relationship between actuation stress and deformation ratio. The results are also grouped in terms of form. The spring form increases the deformation ratio dramatically. The SSC and textile composite actuators show lower actuation stress and deformation performance when stiffer materials (i.e., carbon fiber, glass fiber) are used for the matrix. Freestanding textiles show a similar level of energy density, as most of their volume is occupied by SMA wire.

Figure 7a is a simple comparison of the performance for a single mode of actuation. Still, it cannot fully reflect the various characteristics generated from these forms, as those actuation performances can be varied by the mechanical constraints (Figure 7b), and there are various methods to evaluate them. The curvature or bending angle can help assess the range of deformations a structure of a given length can achieve. Figure 7c compares the bending motion in terms of bending angle and normalized

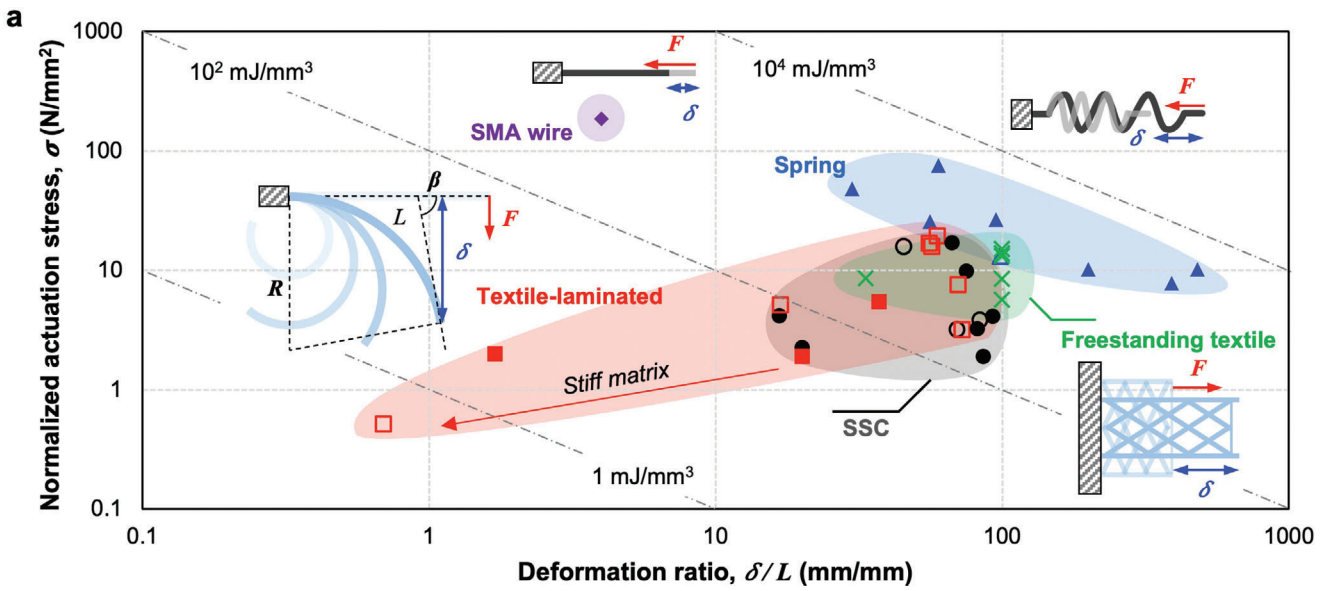

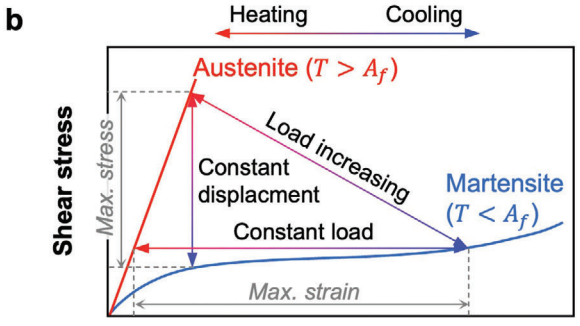

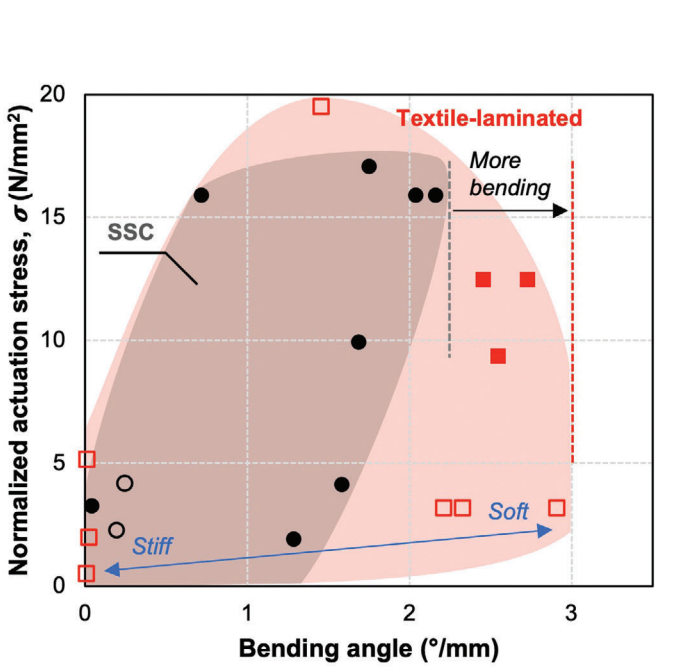

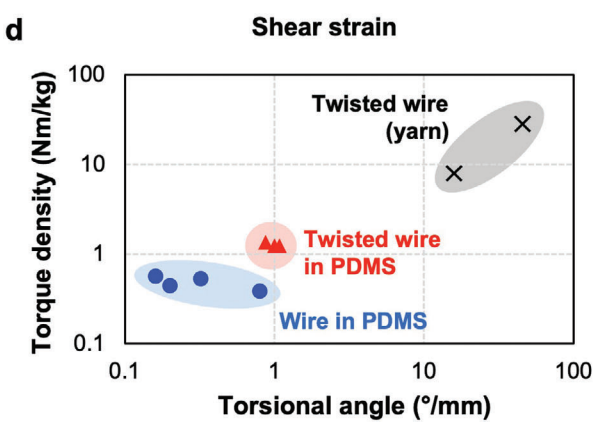

Figure 7. Actuation performances of SMA actuators. a) Comparison of the normalized actuation stress as a function of the deformation ratio between SMA actuators. The actuators are categorized by form (solid marker: the values are indicated in the literature; hollow marker: the values are converted from the literature value).[19,21,24,27,69,77,91,92,103,107,108,114,117–119,125,126,130,138,198,199] b) Stress–strain curves under various boundary conditions (i.e., load increasing, constant displacement, and constant load).[198] c) Comparison of normalized actuation stress as a function of the bending angle. The actuators are categorized by form (solid marker: the values are indicated in the literature; hollow marker: the values are converted from the literature value).[78,85,200,201] d) Comparison of the torque density and rotation of torsional actuators. The actuators are categorized by form (bare twisted SMA wires (yarn), twisted SMA wires in PDMS, and plain wires in PDMS).

actuation stress. When the actuators are grouped in SSC and textile composites, the textile composites exhibit a higher bending angle than SSC actuators. As textile composites have thinner layers than SSC, the lower stiffness enables larger deformations. However, SSC can generate more controlled bending–torsional motions. On the other hand, while the stiff SSC and textile actuators are proper for load-bearing applications, soft ones are proper for large deformation applications.

Furthermore, using Equations (2)–(4), the deflection (δ), curvature (R^{-1}), and bending angle (β) can be converted and vice versa.

Assuming that the bending motion is generated in a perfect circle shape, the relationship between the length of the actuator (L), the bending angle, and the bending radius (R) can be derived by the following relations

$$L = R\beta \tag{2}$$

$$\delta = R(1 - \cos\beta) \tag{3}$$

$$\delta = \frac{L}{\beta}(1 - \cos\beta) \tag{4}$$

where β, R, and δ represent the values to evaluate the displacement performance of bending actuators.

The contraction of the SMA wire placed inside the matrix with offset from the neutral axis generates a moment (M), inducing the deflection of the beam. Assuming that the amount of the deflection caused by the moment is equivalent to that by force applied at the free end of the beam, the tip actuation force (F) can be estimated by the simple beam theory as an action and reaction using Equation (5). The deflection can also be estimated by using the Euler–Bernoulli beam theory assuming a sufficient length-to-width ratio and reasonable deformations by using Equation (6)

$$F = \frac{3M}{2L} \tag{5}$$

$$\delta = \frac{ML^2}{2EI} = \frac{FL^3}{3EI} \tag{6}$$

where E and I are Young's modulus and second moments of area, respectively. These equations are a simple method to get a quick estimate of the performance of different structures to compare them. However, an in-depth study of the theoretical model estimating the shape morphing and actuation force of the SSC actuators should be used to verify these results, which would also require numerical simulations (finite element methods) to reflect the nonlinearity of the soft material and large deformations which may not follow the Euler–Bernoulli beam theory assumptions.

Another property of interest for soft actuators is the ability to have shape retention where a deformation can be maintained after actuator. This can be useful, for example, in a morphing wing where the wing can be morphed into a shape with better aerodynamic performance for a given scenario. Textile composites with epoxy exhibit less actuation force and displacement but have the advantage in shape retention compared to textile composites with PDMS. Interestingly, using a low-temperature melting metal or shape memory polymer can combine shape retention (an advantage of textile composites) and large deformations (an advantage of SSC). The shape is maintained by the high strength of the metal or the polymer but, if necessary, the stiffness decreases by melting the metal or polymer to easily change the shape.

Figure 7d presents a comparison of torsional SMA actuators with different forms. Since these actuators are typically developed from wire-type SMAs, the rotation angle is divided by the length. The torque density is estimated from the total mass of actuators, including the soft matrix. Torsional actuators are grouped into three categories, such as wires in PDMS, twisted wires in PDMS, and twisted wires (yarn). Overall, torque density and rotation have a positive correlation. Twisted wires (yarn) show a higher torque density and rotation since they used two or more wires for fabricating yarn. Twisted wire in PDMS utilizes one wire twisted and embedded in PDMS. The type of wires in PDMS places the wire crossed in the PDMS cuboid.

2.3. Scale

The scale of the SMA element used for actuation can vary from a few micrometers to over a few meters, depending on the intended use. The actuator characteristics vary greatly depending on the size of the SMA element, but the basic behaviors (SME and superelasticity) are preserved even at dimensions as low as the nanometer scale.[96] For example, the most common TSMA, Ni–Ti alloy displays the SME at a thickness of 100 nm,[97] and Cu–Al–Ni is reported that the martensitic transformation phenomenon takes place even under below 50 nm.[98] Also, MSMAs are available to use in small-scale actuation. Reinhold et al.[99] showed that the Ni–Mn–Ga shape recovery effect can be preserved in micrometer scale structures by deformation experiments. Furthermore, as described in Section 2.1.2, the generation of small-scale pores dramatically enhances the MFIS in polycrystalline MSMAs.[63] More information about the effect of geometry and small scale on MSMAs can be found in ref. [60].

2.3.1. Actuation Speed

The low response speed is a challenge for TSMA-based actuators. As reported by Fu et al.,[97] the phase transition of the SMA is completed within several milliseconds. Thus, reducing the time required to reach the phase transition temperature is significant to improve the driving speed of TSMA. In other words, actuation speed is mostly limited by the heating and cooling times. Peirs et al. discussed the scale effects and thermal considerations for microactuators in 1998.[100] When the TSMA is electrically heated up, higher currents can increase the heating speed. When it is cooled down by convection heat transfer, the surface (S) is proportional to the square of the length (L^2), the volume (V) is proportional to L^3, and the convective coefficient (h) is proportional to L^{-1}. Therefore, the thermal response time, $t \propto \frac{V}{S \times h} = \frac{L^3}{L^2 L^{-1}} = L^2$, and the operating frequency (f) is proportional to L^{-2}. This gives an important insight into the scale effect of the SMA actuation. The actuation speed of the SMA would increase significantly as it gets smaller. For example, Lee et al. reported an actuation speed of up to 1.6 kHz when the thickness of the SMA element was reduced to near 1 μm; this is a few orders of magnitude faster than the speeds generally associated with SMA actuators.[24] **Figure 8**a shows the trend of actuation speed by SMA thickness. As depicted in this figure, the smaller the size, the faster the driving speed. Actuation of SMA-based devices is triggered by temperature changes that mediate the phase transitions; actuation speed is limited by the time required for heating and cooling.

However, the scale of the SMA is not the only condition that determines the actuation speed of the SMA-based actuator. In some actuators, a thermal response can be slower or faster due to changes in cooling or heating behaviors. This means that even

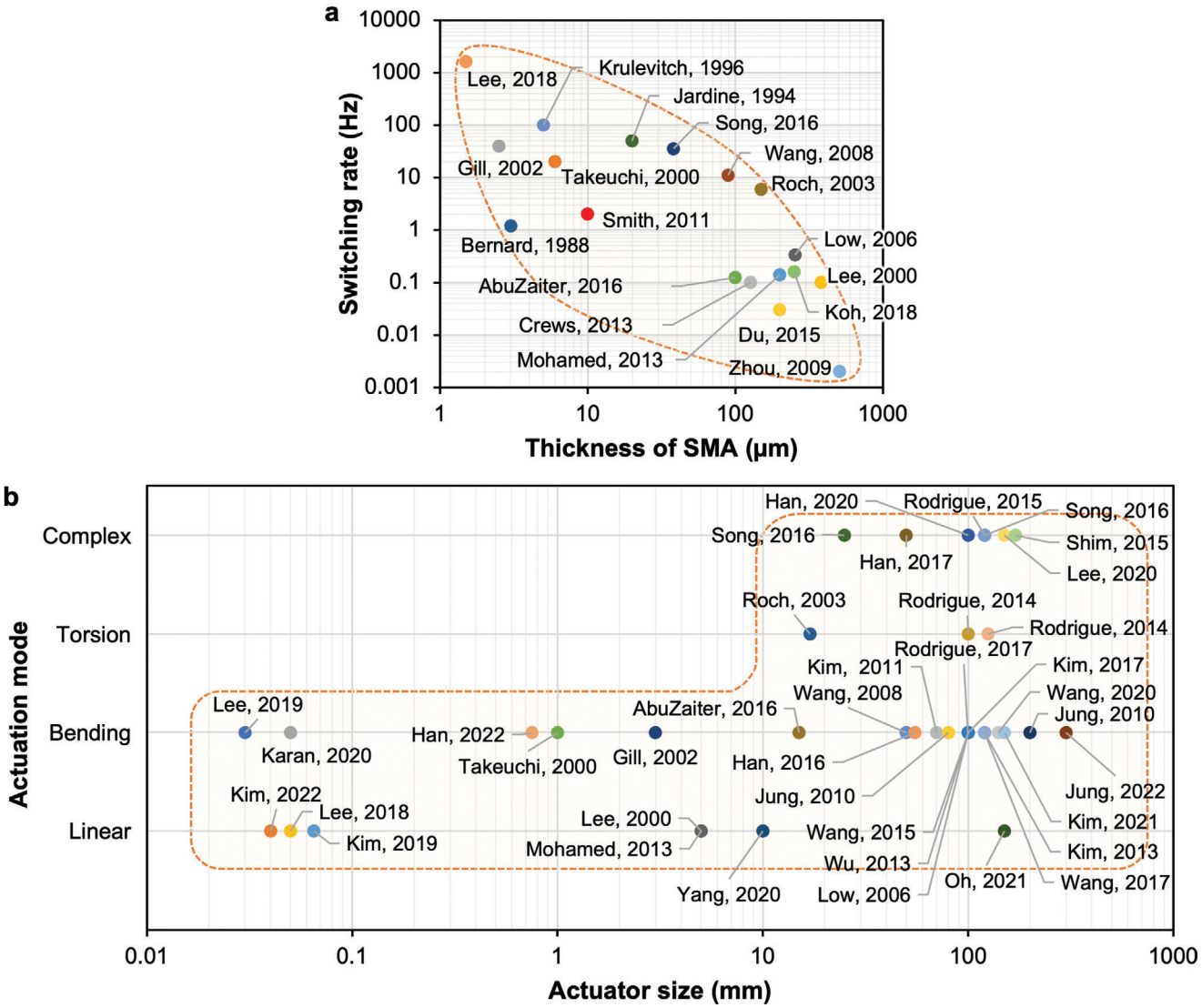

Figure 8. a) Switching rates of SMA actuators according to the thickness of the SMA element. b) Actuation modes according to actuator size. The actuator size indicates the longest dimension of the structure.[19–30,75,88,89,91,101–131]

if actuators have a similar SMA thickness, the driving speeds would vary depending on the size of the entire actuation system or the amount of energy delivered. For example, AbuZaiter et al.[101] in 2016 and Wang et al.[102] in 2008 fabricated actuators using SMA of similar thickness but showed a difference in driving speed of about 100 times. This is because Wang et al. used tens of micrometer wire-type for the SMA area to be heated, while AbuZaiter et al. used sheet-type SMA with a width of several millimeters. Another reason for the different response speeds is mechanical damping caused by additional structures to generate complex deformation modes. They can also cause delays in the temperature response due to the low thermal diffusion. Therefore, in order to gain an advantage from the scale effect for high driving speeds, the entire system design should be comprehensively considered, including the size of actuation components, the control of the applied energy, and the structural materials.

2.3.2. Actuation Mode

In a similar way that the scale affects the actuation speed, Peirs et al. also discussed the scale effect of SMA actuators in terms of force and displacement.[100] If the SMA is operated between the fully detwinned martensite and fully austenite states, the specific work (work per unit volume) is constant, and the work ($F \times d$) is proportional to L^3 since the actuation force (F) of the SMA wire is proportional to L^2, and the displacement (d) is proportional to its length. Thus, linear motion efficiently generates energy and deformation. Likewise, bending actuators can be easily achieved in simple configurations where the SMA element is placed at a fixed eccentricity along the entire length. Thus, the bending motion is also quite efficient as it converts the linear motion into a bending motion.

As shown in Figure 8b, actuators smaller than a few millimeters have been used to implement only linear and bending

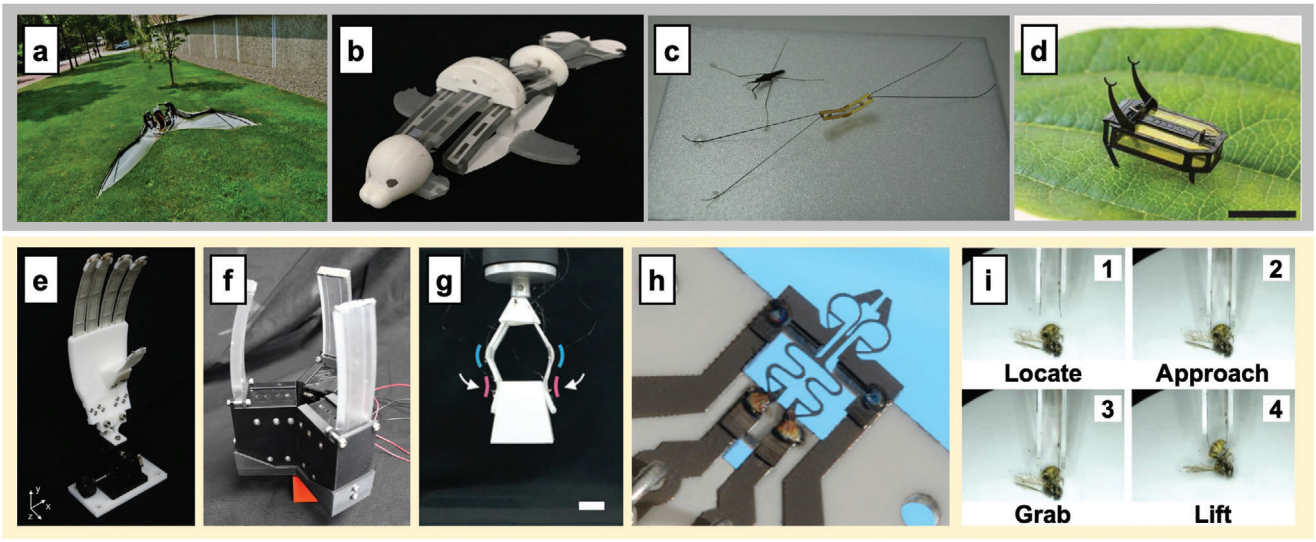

Figure 9. Examples of (a–d) mobile robots and (e–i) robotic multiscale hands. a) An aerial robot. A combination of SMA actuators and electrical motors generates a flapping motion. Reproduced with permission.[148] Copyright 2012, IOP Publishing. b) A seal-mimicking mobile robot. Reproduced with permission.[140] Copyright 2022, Wiley–VCH GmbH. c) A biomimetic water strider robot. Reproduced with permission.[145] Copyright 2015, AAAS. d) A RoBeetle powered by methanol (scale bar: 10 mm). Reproduced with permission.[71] Copyright 2020, AAAS. e–g) SSC-actuator-based grippers (scale bar: 30 mm). Reproduced with permission.[123] Copyright 2017, Mary Ann Liebert, Inc. Reproduced with permission.[150] Copyright 2019, Springer Nature. Reproduced with permission.[151] Copyright 2016, Elsevier. h) A micro-SMA gripper. Reproduced with permission.[155] Copyright 2002, Elsevier. i) A SSC-actuator-based microgripper. Reproduced with permission.[156] Copyright 2020, Wiley–VCH GmbH.

modes, whereas actuators larger than a few millimeters can also produce torsional and complex deformations. Compared to linear and bending motions, it is difficult to demonstrate torsional motions at the microscale due to not only the nature of the wire-type SMA but also physical and manufacturing limitations. For example, when one tries to make a torsional motion using a SMA wire, two approaches are available which are similar to that of torsional actuator designs at the mesoscale. One is applying the shear strain along the wire by twisting the wire. However, the strain distribution is decreased in a radial axis; thus, the center has twinned martensite and the surface has detwinned martensite. It lowers actuation performance, as martensitic transformation does not fully happen in the entire volume (Figure S2, Supporting Information). For the same reason, this approach is inefficient to generate complex motions. Another method is using additional frames to provide an offset between the force axis and neutral axis. The offset helps the linear contraction of the SMA to generate torque. Although this system design enables efficient torsional and complex motions, the practical implementation is limited by fabrication challenges, such as manufacturing and assembly of complex composite architectures at small scales. Additionally, this concept has a limitation in miniaturization because adding a frame increases the size of the actuator itself.

The implementation of novel design and MEMS fabrication techniques can tackle the problems of embedding SMAs into composite forms, generating torsional and complex motion. This integration requires precise positioning of the SMA element within a larger (but still relatively small) structure. Wet etching can enhance the production rate of small-scale and patterned SMA structures. Also, the photolithography and deposition processes can join soft or hard materials with SMAs (such as a compliant frame or bimetallic design).[132] Although the above approaches allow small SMAs to exhibit high actuation speeds and various actuation modes, precise motion and force control still remain challenging. Compared to lead zirconate titanate (PZT) actuators, which are representative of small-scale actuators, SMAs are lacking in terms of precise control and a simple powering system. Therefore, future development of design, control, material, and fabrication techniques can expand the application of small-scale SMA actuators.

3. Discussion

3.1. Applications

SMAs have found many applications at a wide range of scales; tailored designs exploit the unique properties of SMAs, for example, in mobile robots (crawling,[71,133–139] water-based,[77,140–144] jumping,[145–147] and flying robots;[148,149] **Figure 9**a–d). One of the main motivations for using SMAs in such applications ar their high-power density along with only requiring electrical power for powering them through Joule heating. This means that the weight of the structure can be minimized while still producing powerful motions. Such robots have also been used for gripping (Figure 9e–i) at both the meso-[69,122,123,150–154] and microscales.[155,156] At the mesoscale, SMA-based grippers are generally composite structures that produce the smooth bending deformations usually seen in soft robotic grippers. The combination of smooth deformation and reasonable force makes SMA actuators suitable for soft grasping as they do not require a pneumatic energy source.

SMAs have also recently been applied in wearable devices (**Figure 10**a–c). SMA wires woven into textiles have been used to make compression garments,[157] self-conformable shoes,[158]

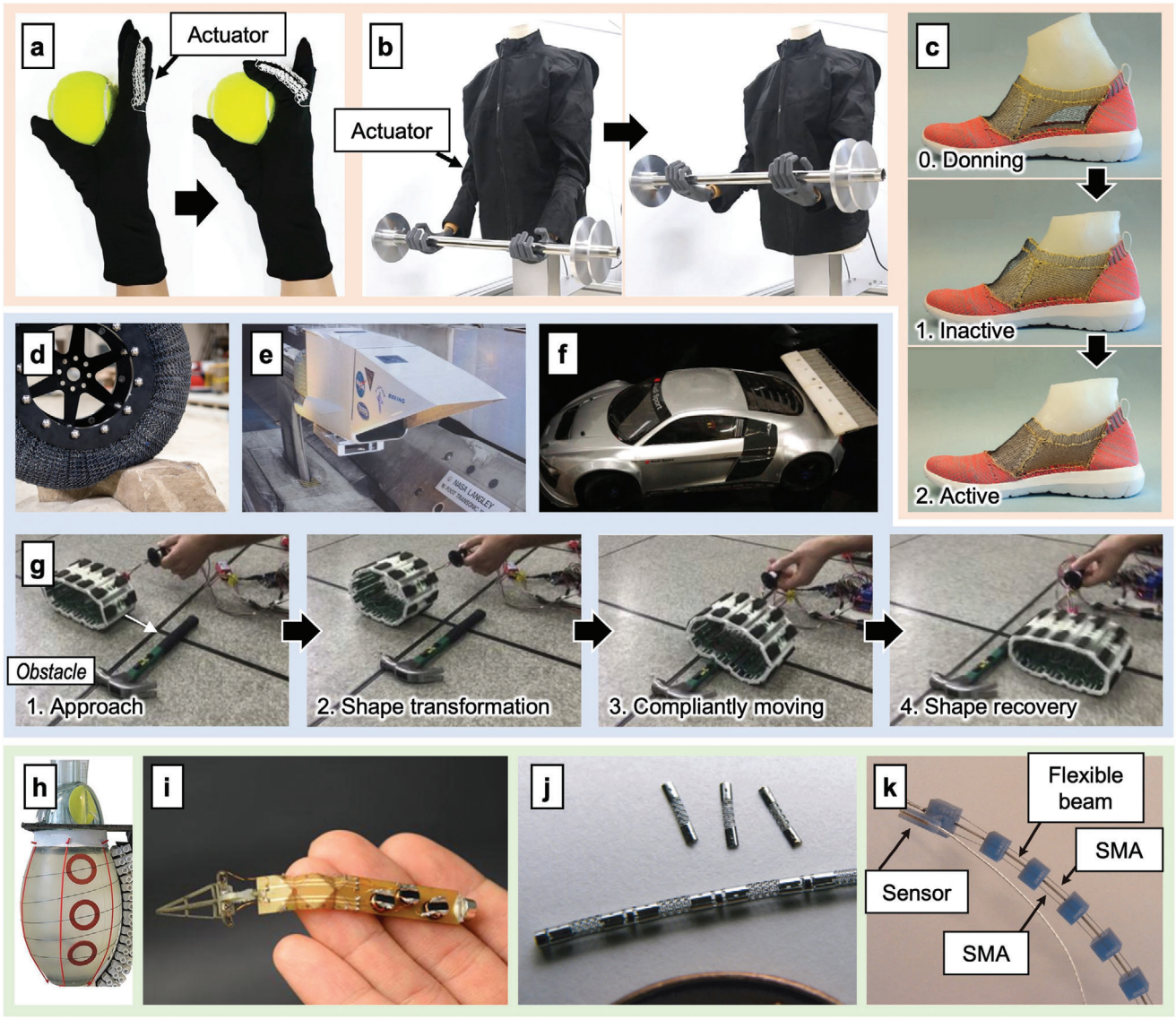

Figure 10. Examples of (a–c) wearable devices; (d–g) aerospace/automotive applications; and (h–k) biomedical devices. a) A wearable SMA exoglove. Reproduced with permission.[162] Copyright 2022, Springer Nature. b) SMA clothes that aid load carrying. Reproduced with permission.[159] Copyright 2019, Springer Nature. c) A SMA shoe fastener. Reproduced with permission.[158] Copyright 2021, Wiley–VCH GmbH. d,g) Adjustable automotive wheels that can climb random obstacles. Reproduced with permission.[166] Copyright 2022, NASA. Reproduced with permission.[174] Copyright 2020, Elsevier. e) A smart engine inlet. Reproduced with permission.[165] Copyright 2003, SAGE Publications. f) A morphing spoiler. Reproduced with permission.[90] Copyright 2016, Elsevier. h) A Fontan circulation device for cardiac assistance. Reproduced with permission.[172] Copyright 2013, IUPESM. i) A wireless robotic arm. Reproduced with permission.[170] Copyright 2017, AAAS. j,k) Active catheters. Reproduced with permission.[167] Copyright 2012, SAGE Publications. Reproduced with permission.[168] Copyright 2008, Elsevier.

movement assistance devices,[159,160] and soft exogloves.[161–163] In the transportation field (Figure 10d–g), SMAs have been employed to fabricate smart aircraft engine inlets,[164] morphing airfoils,[165] and (airless) superelastic wheels.[166] For such large-scale applications, the devices are generally powered by waste heat or operate in a superelastic state. SMAs have found many applications in the biomedical field (Figure 10h–k); SMA-based self-expanding stents are common, but SMAs are also found in active catheters,[167–169] wireless tools,[170] endoscopes,[171] Fontan circulation devices for cardiac assistance,[172] and cardiac resynchronization therapy devices.[173]

3.2. Limitations

However, SMA actuators still have certain limitations. Most recent research on SMA materials focused on twin boundary shift (or phase changes) and transformation temperatures using differential scanning calorimetry and crystal structure analyses; actuation strain was not measured. The lack of such data restricts the development of actuators using newer materials; it is unclear whether they merit investigation. Collaborations between material scientists and actuator engineers are required. Also, as nitinol is a high-performance

SMA, hybridization of nitinol with other materials is worth exploring.

The actuation cycle of TSMAs also represents another significant limitation as they have to be heated, change phase, and cool down entirely to actuate and return to their original state. This significantly limits possible applications; a single SMA can only produce a single motion. The addition of a metasurface may overcome this limitation. When the surface of a micro-SMA actuator is patterned at the sub-microscale, the light absorption rate at a specific wavelength can be optimized to allow laser driving. When the surface has different patterns, it is possible to control actuation by varying the laser wavelengths. This greatly enhances the utility of SMA actuators.

Another limitation is that the geometry of SMA actuators is restricted to wire, sheet, and wire-based 3D structures. The development of 3D printable SMAs can diversify the form of SMA structures.[175] Recent advances in the field of 3D printing have enabled the 3D printing of TSMAs made from Ni–Ti-based and Cu-based alloys.[176] Similarly, 3D-printed MSMA structures made from Ni–Mn–Ga alloys have been reported.[177] However, these 3D printable SMAs still have limitations in use due to insufficient shape memory effect, low repeatability, and low reversibility. Thus, several recent approaches aim to resolve them, such as tuning the material composition, decreasing the impurity,[178] and improving the 3D printing accuracy.[179,180] Eventually, implementing 3D-printed SMA structures could diversify the form of the SMA actuators at all scales and help with the fabrication of complex composite structures even at small scales. This will have a significant effect on the use of SMAs.

Mesoscale, SMA-based soft robotic grippers remain inferior to pneumatic grippers in terms of grasping performance. The former grippers are associated with degradation of the polymer matrix around the interface with SMA wires, SMA degradation with sustained use, and weak grasping forces. These issues can be resolved by decoupling the SMA length from that of the volume to be deformed. Also, SMA degradation under sustained use can be partially resolved by improving actuator heat management, by exploiting the self-sensing properties of SMAs. Unresolved issues include matrix degradation around SMA wires (where stress is concentrated) and the large differences in Young's modulus among SMAs. Multimaterial designs and changes in SMA–matrix interactions may resolve these problems. Placement of SMA wires within tubes embedded in polymers may be helpful. When these issues are solved, the performance and longevity of SMA-based soft robotic grippers may approach those of current grippers using tethered pneumatic sources.

Furthermore, textile actuators, which can be utilized for wearable applications require an ergonomic design, be comfortable for the wearer, be capable of complex shape morphing, and have specific functions for a given usage. Thus, clothing using textile actuators is usually used as a special-purpose garment. For example, it can be used for rehabilitation or for astronauts. In many cases, SMA clothing used in these fields is used as a compression garment, but in medical practice, it is used for simple therapy without any dynamic motions. Also, a functional design should make the garment highly wearable, but they are currently significantly more inconvenient to put on and take off than regular clothes. In the case of NASA's project, they developed compression garments for astronauts, but wearability analysis is required for practical applications.[181,182] In addition, numerous ergonomic factors should be accompanied, such as joint flexion, muscle orientation, and human-wearable device interactions. Including aesthetic design, significant research to improve the quality and usability of such smart garments will be necessary to make them practical in daily life.

At smaller scales, SMA actuators produce simple linear and bending motions, attributable to limitations in manufacturing. SMAs are difficult to produce at this scale and it is challenging to pair them with structures possessing the anisotropic properties required for complex deformations. Advances in the microfabrication of both SMAs and supporting materials will solve such issues. For example, a microscale scaffold could be fabricated via electrohydrodynamic printing or two-photon lithography and used to form a microscale SSC with anisotropic properties allowing for complex deformations. The advances in the 3D printing of SMA elements should also allow for the free-form fabrication of actuators at this scale and facilitate the manufacturing of small-scale structures with complex configurations and thus complex functionalities.

Additionally, improving small-scale SMA production methods is required to facilitate their implementation in various applications. Laser is used for machining and welding, which are conventional and high-throughput processes but not suitable for SMA shaping at a small scale. Even though a nanosecond laser can be used for processing, the heat-affected zone (HAZ) would be significant in microscale structures. Exposure to high temperatures (over the A_f) over long periods makes the SMA lose its SME. Likewise, the HAZ can damage the crystalline structures for martensitic transformation. Electrical discharge machining is another method for shaping but is limited to fabricating under 100 μm size of the feature.

Also, the miniaturization of SMA has a feature size limit (≈50 nm). When the structure size decreases under 50 nm, the SME is attenuated. Therefore, it may be worthwhile to consider adopting other smart materials for smaller scale actuation. Recently, a novel microscale shape memory actuator has been developed for microrobotic applications, creating a strain in the oxidized layer that causes bending motion by electric energy.[183] Also, 30 nm thin ferroelectric–ferromagnetic ceramic composites exhibit shape memory behavior.[184] As nanomagnets can demonstrate programmed shape generation, they are also a promising method for small-scale actuation sources.[185]

Hydrogel-based actuators also present significant promise, especially for miniaturized devices, due to their simpler manufacturing process and ability to achieve complex designs. Stimuli-responsive hydrogels, which change their volume in response to external stimuli (i.e., heat, pH, electricity, or light), can generate self-walking or crawling motions.[186,187] These hydrogels can also be used to create shape morphing,[188,189] programmable,[190,191] or transformable gels.[192] Additionally, the addition of magnetic nanoparticles to stimulus-responsive hydrogels enables navigation with gripping of organic objects[193,194] or grasping tissue within the gastrointestinal (GI) tract.[195] Besides, polymer/gel-based thin-film bilayers can be used for triggered residual-stress-based actuators, making them suitable for applications such as biopsy, drug delivery, or microinjection.[196,197] These polymeric materials can be photocurable and easily manufactured into

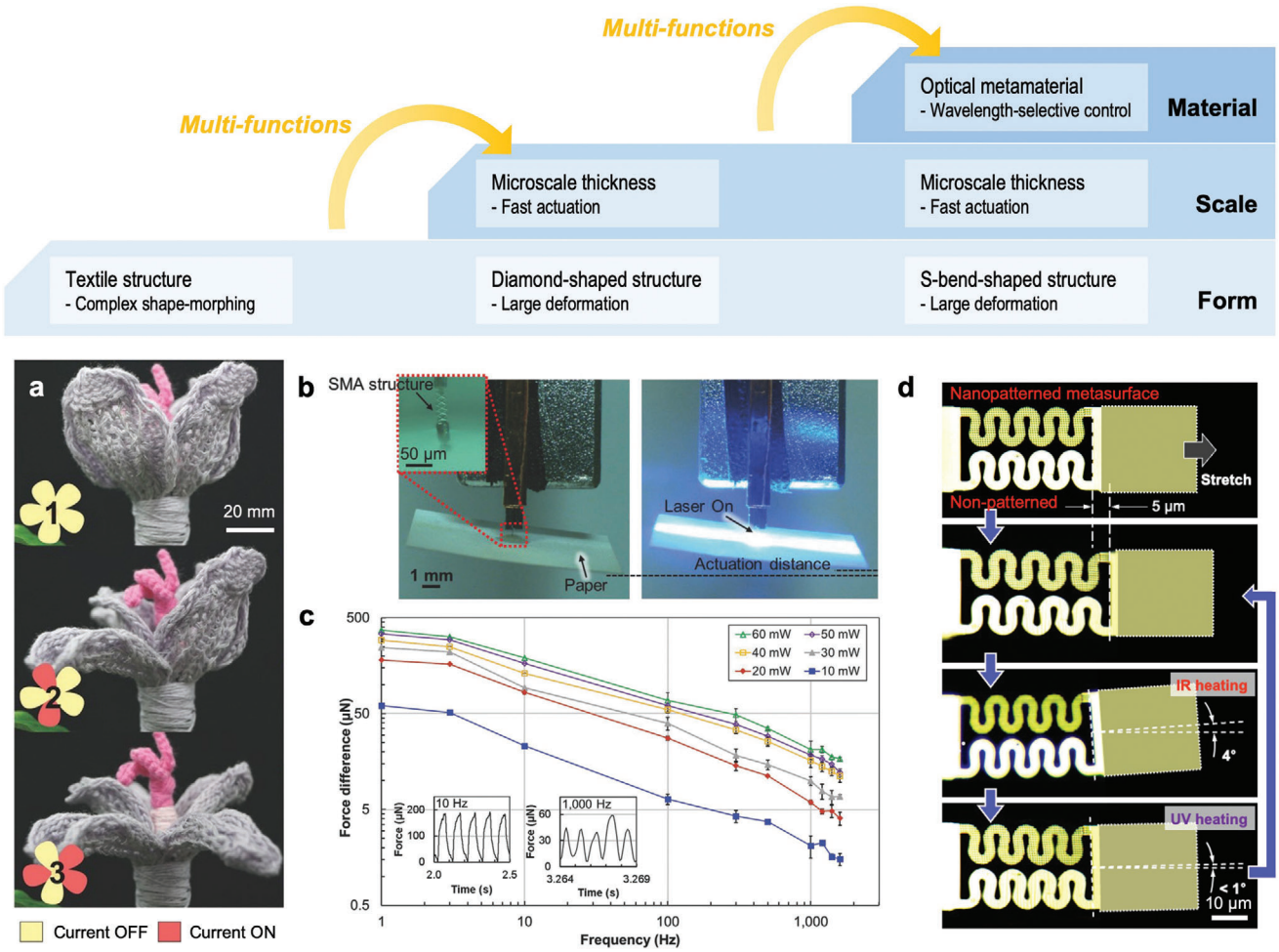

Figure 11. Examples of how form, scale, and material allow for multifunctionality and improve the performance of SMA actuators. a) The knit actuator form makes it possible to demonstrate large deformations using SMA wire contraction. Reproduced with permission.[92] Copyright 2017, Wiley–VCH GmbH. b,c) By adding the scale effect, the cooling speed can be increased dramatically. The diamond-shaped design was capable of large deformations and its scale effect allowed it to achieve an actuation speed of 1.6 kHz. Reproduced with permission.[24] Copyright 2018, Wiley–VCH GmbH. d) The light absorptance can be tailored through surface treatments to enable to SMA to selectively absorb the IR light. The microscale S-shaped SMA actuator showed high deformation and fast cooling, and the use of IR and UV heating enabled sequential deformations. Reproduced with permission.[21] Copyright 2022, Wiley–VCH GmbH.

complex 3D structures at smaller scales by stereolithographic 3D printing methods.

We summarize the actuation properties of these various actuation sources in Table S1 (Supporting Information), to assist engineers in selecting the most suitable actuation source for their application. It is important to note that each actuation source has its unique strengths and limitations, and the selection should be based on the specific requirements of the intended application.

3.3. Outlook

Although there are limitations in terms of practical applications, recent achievements in the field have shown that the development of SMA considering the material, form, and scale features can significantly advance the performance of SMA actuators. Further integration and synergies among these aspects will enable the development of highly functional structures with high potential for pioneering applications. For instance, **Figure 11** shows how the integration of material, form, and scale advances could enable the development of a multifunction actuator. Improvements in form can help in smooth motions or producing more complex formations (Figure 11a). However, when the scale effects are added to this designed form, the actuator can gain additional characteristics such as large deformation and fast actuation (Figure 11b,c). Moreover, through material tuning, such as surface treatment to obtain an optical metasurface, light with different wavelengths can be used to control different portions of the structure to enable sequential motions (Figure 11d). A combination of MSMA and TSMA can be used to derive multistimulus-responsive actuators that can achieve multiple actuation modes. If composite-based designs are employed here, then the bending and torsional motions could be produced independently and demonstrated at the microscale. Thus, the synergy of material,

form, and scale would enable complex motions at the small scale or the continuous shape morphing for multimode actuation. As a result, these multifunctionality SMA actuators can be used to broaden their applicability for real-life applications.

We also suggest five major challenges that can serve as technical guidelines for developing SMA actuators in the next decade. These challenges are as follows.

3.3.1. Precise and Uniform SMA Material Fabrication

The actuation performance of SMA is highly sensitive to its material composition and postprocessing parameters. Even subtle differences in material composition can result in significant variations in actuation performance, including A_f transformation temperature and actuation strain. Currently, mass production lacks adequate precision to achieve uniform performance, resulting in low repeatability and limiting the widespread use of SMA. To address this issue, there is a need for precise quality control of actuation performance at the level of three sigma (99.7% of products have the same actuation behavior) or higher. Achieving this level of precision in material fabrication is crucial to ensure consistent and reliable performance of SMA, making them more widely applicable in various devices.

3.3.2. Increasing the Maximum Actuation Strain of MSMAs

While various approaches have been developed to tackle the limitation of small actuation strain in MSMAs, the maximum strain capacity of these materials still requires further improvement. In order to expand the use of MSMAs, it is necessary to achieve a similar strain range to TSMAs, such as 4–6%. Furthermore, it would be beneficial to develop mass production methods to facilitate their widespread use.

3.3.3. More Stable SSC Actuator and Softer Textile Actuator

SSCs have great potential for their use as soft actuators with high-degree-of-freedom motion. However, the reliability of the actuator is currently insufficient for many practical applications. To enable their widespread use, it is necessary to achieve a high level of repeatability, with a target of 10^6–10^7 under significant load. Similarly, textile actuators hold promise for wearable devices, but the high stiffness of metal fibers can make it difficult to generate curved structures. Additionally, the low compatibility in stiffness between the textile and alloy materials can limit their processability. Thus, addressing these challenges through innovative material design and manufacturing techniques is required to achieve the full potential of SSC and textile actuators.

3.3.4. 3D Structure Fabrication

While the manufacturing process for wire (1D)- or planar (2D)-type SMA actuators has been well established through methods such as drawing, rolling, sputtering, and assembly, the potential for 3D printing to produce SMA actuators is still largely unexplored. The fabrication of fully 3D SMA actuators can enable new actuation modes and facilitate their miniaturization. Thus, it will be necessary to demonstrate the shape memory effect in 3D-printed structures with a resolution of at least 0.1 mm. The accomplishment of this milestone within the next decade could pave the way for innovative avenues in the design and fabrication of complex SMA actuator geometries. This, in turn, has the potential to unlock novel functionalities and applications, thus opening up a world of new possibilities.

3.3.5. Miniaturization

Although several demonstrations have shown miniaturized SMA actuators in robots with a size of around 1 cm^3, further miniaturization is necessary at the sub-1 cm^3 level. Complex assembly in 1 mm^3 of size is another challenge for miniaturization to perform complex motions. Furthermore, the manufacturing process of wire-shaped actuators needs to be improved to enable the fabrication of fiber diameters in the range of 1 μm for smaller-scale applications.

In addition to the major challenges discussed earlier, there are several minor challenges that need to be addressed. One of these challenges is to develop materials that can achieve high-cycle stability, low-temperature hysteresis, and low manufacturing costs. Another challenge is to explore the combination of multistimuli (thermal, magnetic, and radio frequency (RF)) actuators, which can provide different actuation modes. To achieve high power efficiency and actuation speeds, micro-/nanoscale structure designs and multilayer coatings are suggested as potential solutions.

Moreover, we recommend evaluating SMA actuators comprehensively by the methods proposed in this review. To date, the lack of common evaluation methods for SMA actuators poses a challenge in comparing their performance. Therefore, adopting a common evaluation standard or criteria would provide guidance to improve the performance of SMA actuators and promote further advances in the field.

4. Conclusion

SMA actuators are a wide family of smart materials of different chemical nature each with their own operating temperature ranges and actuation characteristics. They can be processed into different forms and display diverse actuation modes, and can operate at a wide range of scales. While SMAs have unique advantages that could allow them to replace conventional actuators in many applications, significant improvements are required prior to their further commercialization. We have identified the unique synergies in terms of material, form, and scale which can enable SMAs to become multifunctional intelligent machines. Further development on each of these three individual aspects as well as developing novel synergies between them will allow imbuing SMA actuators with a high level of physical intelligence, while enabling their use in both domestic objects and highly specialized devices at all scales.

Supporting Information

Supporting Information is available from the Wiley Online Library or from the author.

Acknowledgements

This work was supported by the National Research Foundation of Korea (NRF) grants funded by the MSIT (Grant Nos. NRF-2021R1A2B5B03087094, NRF-2021R1A4A2001824, NRF-2020R1A4A1018227, NRF-2020R1G1A1099734, NRF-2018R1A5A7023490), the Korea Institute of Machinery and Materials (KIMM) funding (Grant No. NK236C). S.P. acknowledges an ERC Consolidator Grant "Highly Integrated Nanoscale Robots for Targeted Delivery to the Central Nervous System" (HINBOTS), Grant No. 771565. M.-S.K. acknowledges partial financial support by the Swiss National Science Foundation under Project No. 200021L_197017. This work was also supported by INHA UNIVERSITY Research Grant.

Open access funding provided by Eidgenossische Technische Hochschule Zurich.

Conflict of Interest

The authors declare no conflict of interest.

Keywords

composite materials, scale effects, shape memory alloys, soft actuators, soft robotics

Received: September 16, 2022
Revised: April 11, 2023
Published online: June 29, 2023

[1] A. Ölander, *J. Am. Chem. Soc.* **1932**, *54*, 3819.
[2] L. C. Chang, T. Read, *JOM* **1951**, *3*, 47.
[3] T. Tadaki, K. Otsuka, K. Shimizu, *Annu. Rev. Mater. Sci.* **1988**, *18*, 25.
[4] W. J. Buehler, R. C. Wiley, *The Properties of TiNi and Associated Phases*, Naval Ordnance Lab, White Oak, MD **1961**.
[5] C. Mavroidis, C. Pfeiffer, M. Mosley, in *Automation, Miniature Robotics, and Sensors for Nondestructive Testing and Evaluation*, Vol. *4*, NASA, USA **2000**, p. 189.
[6] D. Stöckel, *Proc.: Shape Memory Alloys for Power Systems*, Electric Power Research Inst., USA, Vol. *1*, **1995**, p. 1.
[7] S. Mohan, A. Banerjee, *Smart Mater. Struct.* **2021**, *30*, 055011.
[8] B. T. Lester, T. Baxevanis, Y. Chemisky, D. C. Lagoudas, *Acta Mech.* **2015**, *226*, 3907.
[9] T. W. Duerig, J. Albrecht, G. H. Gessinger, *JOM* **1982**, *34*, 14.
[10] T. Hoshiya, F. Takada, Y. Ichihashi, H.-R. Pak, *Mater. Sci. Eng., A* **1990**, *130*, 185.
[11] H. Kahn, M. Huff, A. Heuer, *J. Micromech. Microeng.* **1998**, *8*, 213.
[12] L. M. Schetky, *Mater. Des.* **1991**, *12*, 29.
[13] L. Brinson, R. Lammering, *Int. J. Solids Struct.* **1993**, *30*, 3261.
[14] K. Safaei, H. Abedi, M. Nematollahi, F. Kordizadeh, H. Dabbaghi, P. Bayati, R. Javanbakht, A. Jahadakbar, M. Elahinia, B. Poorganji, *JOM* **2021**, *73*, 3771.
[15] V. Malik, S. Srivastava, S. Gupta, V. Sharma, M. Vishnoi, T. Mamatha, *Mater. Today: Proc.* **2021**, *44*, 4961.
[16] R. Chaudhari, J. J. Vora, D. Parikh, *Recent Adv. Mech. Infrastruct.* **2021**, 123.
[17] A. Riccio, S. Saputo, M. Zarrelli, A. Sellitto, C. Napolitano, V. Acanfora, presented at *2021 IEEE 8th Int. Workshop Metrology AeroSpace (MetroAeroSpace)*, Italy, June, **2021**.
[18] N. Kalashnikov, C. Moraes, *Adv. Funct. Mater.* **2019**, *29*, 1903327.
[19] M.-W. Han, M.-S. Kim, S.-H. Ahn, *Composites, Part B* **2020**, *198*, 108170.
[20] W.-K. Jung, S.-M. Lee, S.-H. Ahn, J. Park, *J. Ind. Text.* **2022**, *51*, 1989S.
[21] M. S. Kim, H. S. Lee, Y. Cho, J. K. Heo, Y. J. Quan, S. W. Lee, H. J. Pahk, S. H. Ahn, *Adv. Opt. Mater.* **2022**, *10*, 2102024.
[22] M. S. Kim, H. T. Lee, S. H. Ahn, *Adv. Mater. Technol.* **2019**, *4*, 1900583.
[23] H.-T. Lee, K.-I. Lee, K.-H. Jang, S.-H. Ahn, *Int. J. Precis. Eng. Manuf.* **2020**, *21*, 491.
[24] H. T. Lee, M. S. Kim, G. Y. Lee, C. S. Kim, S. H. Ahn, *Small* **2018**, *14*, 1801023.
[25] S.-M. Lee, W.-K. Jung, S.-H. Ahn, J. Park, presented at *Int. Textile Apparel Association Annual Conf. Proc.*, Virtual, November, **2020**.
[26] S.-H. Song, J.-Y. Lee, H. Rodrigue, I.-S. Choi, Y. J. Kang, S.-H. Ahn, *Sci. Rep.* **2016**, *6*, 21118.
[27] R. Wu, M.-W. Han, G.-Y. Lee, S.-H. Ahn, *Smart Mater. Struct.* **2013**, *22*, 125007.
[28] B.-S. Jung, M.-S. Kim, J.-S. Kim, Y.-M. Kim, W.-Y. Lee, S.-H. Ahn, *Phys. Scr.* **2010**, *T139*, 014042.
[29] B.-S. Jung, J.-P. Kong, N. Li, Y.-M. Kim, M.-S. Kim, S.-H. Ahn, M. Cho, *J. Intel. Mater. Syst. Struct.* **2013**, *24*, 89.
[30] B. S. Jung, M. S. Kim, Y. M. Kim, S. H. Ahn, *Materialwiss. Werkstofftech.* **2010**, *41*, 320.
[31] S. Akbari, A. H. Sakhaei, S. Panjwani, K. Kowsari, Q. Ge, *Sens. Actuators, A* **2021**, *321*, 112598.
[32] M. M. Hasan, T. Baxevanis, *J. Intell. Mater. Syst. Struct.* **2022**, *33*, 1475.
[33] K. Safaei, M. Nematollahi, P. Bayati, H. Dabbaghi, O. Benafan, M. Elahinia, *Eng. Struct.* **2021**, *226*, 111383.
[34] M. Hao, J. Li, S. Park, S. Moura, C. Dames, *Nat. Energy* **2018**, *3*, 899.
[35] P. Hua, M. Xia, Y. Onuki, Q. Sun, *Nat. Nanotechnol.* **2021**, *16*, 409.
[36] S. I. H. Shah, A. Sarkar, R. Phon, S. Lim, *Adv. Opt. Mater.* **2020**, *8*, 2001180.
[37] O. Benafan, National Aeronautics and Space Administration, 2022, https://shapememory.grc.nasa.gov/ (accessed: May **2022**).
[38] J. Ma, I. Karaman, *Science* **2010**, *327*, 1468.
[39] O. Benafan, G. S. Bigelow, A. W. Young, *Adv. Eng. Mater.* **2020**, *22*, 1901370.
[40] K. Otsuka, C. M. Wayman, in *Shape Memory Materials*, Cambridge University Press, Cambridge **1999**.
[41] J. Frenzel, E. P. George, A. Dlouhy, C. Somsen, M.-X. Wagner, G. Eggeler, *Acta Mater.* **2010**, *58*, 3444.
[42] Y. Tanaka, Y. Himuro, R. Kainuma, Y. Sutou, T. Omori, K. Ishida, *Science* **2010**, *327*, 1488.
[43] Y. H. Wen, H. B. Peng, D. Raabe, I. Gutiérrez-Urrutia, J. Chen, Y. Y. Du, *Nat. Commun.* **2014**, *5*, 4964.
[44] L. Tseng, J. Ma, S. Wang, I. Karaman, M. Kaya, Z. Luo, Y. Chumlyakov, *Acta Mater.* **2015**, *89*, 374.
[45] C. Lexcellent, *Shape-Memory Alloys Handbook*, John Wiley & Sons, Hoboken, NJ **2013**.
[46] X. Yang, L. Ma, J. Shang, *Sci. Rep.* **2019**, *9*, 3221.
[47] A. Khandelwal, V. Buravalla, *Int. J. Struct. Changes Solids* **2009**, *1*, 111.
[48] P. Nnamchi, A. Younes, S. González, *Intermetallics* **2019**, *105*, 61.
[49] B. S. Shariat, Q. Meng, A. S. Mahmud, Z. Wu, R. Bakhtiari, J. Zhang, F. Motazedian, H. Yang, G. Rio, T.-h. Nam, *Mater. Des.* **2017**, *124*, 225.
[50] K. Mehta, K. Gupta, *Fabrication and Processing of Shape Memory Alloys*, Springer International Publishing, Berlin **2019**.
[51] Y. Suzuki, K. Otsuka, C. M. Wayman, in *Shape Memory Materials*, Cambridge University Press, Cambridge, England **1998**, p. 133.
[52] K. Ullakko, *J. Mater. Eng. Perform.* **1996**, *5*, 405.

[53] E. Pagounis, R. Chulist, M. Szczerba, M. Laufenberg, *Scr. Mater.* **2014**, *83*, 29.
[54] A. Pérez-Checa, J. Feuchtwanger, J. Barandiaran, A. Sozinov, K. Ullakko, V. Chernenko, *Scr. Mater.* **2018**, *154*, 131.
[55] V. Chernenko, E. Cesari, V. Kokorin, I. Vitenko, *Scr. Metall. Mater.* **1995**, *33*, 1239.
[56] Y. Boonyongmaneerat, M. Chmielus, D. C. Dunand, P. Müllner, *Phys. Rev. Lett.* **2007**, *99*, 247201.
[57] J. Wang, H. Bai, C. Jiang, Y. Li, H. Xu, *Mater. Sci. Eng., A* **2010**, *527*, 1975.
[58] P.-P. Li, J.-M. Wang, C.-B. Jiang, *Chin. Phys. B* **2011**, *20*, 028104.
[59] X. Zhang, M. Qian, X. Zhang, M. Qian, *Applicatio,n of Magnetic Shape Memory Alloys*, Springer Singapore, Singapore **2022**.
[60] D. C. Dunand, P. Müllner, *Adv. Mater.* **2011**, *23*, 216.
[61] Z. Li, Z. Li, B. Yang, X. He, W. Gan, Y. Zhang, Z. Li, Y. Zhang, C. Esling, X. Zhao, L. Zuo, *Mater. Sci. Eng., A* **2020**, *780*, 139170.
[62] H. Shi, Z. Liu, H. Wang, X. Mei, *Adv. Mech. Eng.* **2021**, *13*, https://doi.org/10.1177/16878140211016985.
[63] M. Chmielus, X. X. Zhang, C. Witherspoon, D. C. Dunand, P. Müllner, *Nat. Mater.* **2009**, *8*, 863.
[64] A. Likhachev, A. Sozinov, K. Ullakko, *Mech. Mater.* **2006**, *38*, 551.
[65] M. Lee, S. Lee, S. Lim, *Sensors* **2021**, *21*, 3026.
[66] Y. Yu, C. Zhang, Z. Han, M. Zhou, *IEEE Trans. Magn.* **2021**, *57*, 4001604.
[67] C. Feng, S. Wang, L. Yin, X. Li, M. Yao, F. Yang, X. Tang, L. Wang, W. Mi, G. Yu, *Adv. Funct. Mater.* **2018**, *28*, 1803335.
[68] V. R. Guiza-Arguello, J. A. Monroe, I. Karaman, M. S. Hahn, *J. Biomed. Mater. Res., Part B* **2016**, *104*, 853.
[69] S. Oh, R. Tabassian, P. Thangasamy, M. Mahato, V. H. Nguyen, S. Nam, Z. Huapeng, I. K. Oh, *Adv. Funct. Mater.* **2021**, *32*, 2111145.
[70] M. Sivaperuman Kalairaj, H. Banerjee, C. M. Lim, P.-Y. Chen, H. Ren, *RSC Adv.* **2019**, *9*, 34244.
[71] X. Yang, L. Chang, N. O. Pérez-Arancibia, *Sci. Rob.* **2020**, *5*, eaba0015.
[72] S. Zaidi, F. Lamarque, C. Prelle, O. Carton, A. Zeinert, *Smart Mater. Struct.* **2012**, *21*, 115027.
[73] S. Jin, Y. Zhang, Q. Wang, D. Zhang, S. Zhang, *Colloids Surf., B* **2013**, *101*, 343.
[74] I. Aaltio, X. Liu, M. Valden, K. Lahtonen, O. Söderberg, Y. Ge, S.-P. Hannula, *J. Alloys Compd.* **2013**, *577*, S367.
[75] J.-E. Shim, Y.-J. Quan, W. Wang, H. Rodrigue, S.-H. Song, S.-H. Ahn, *Smart Mater. Struct.* **2015**, *24*, 125033.
[76] J. Sheng, D. Gandhi, R. Gullapalli, J. M. Simard, J. P. Desai, *IEEE Trans. Rob.* **2016**, *33*, 240.
[77] S.-H. Song, M.-S. Kim, H. Rodrigue, J.-Y. Lee, J.-E. Shim, M.-C. Kim, W.-S. Chu, S.-H. Ahn, *Bioinspiration Biomimetics* **2016**, *11*, 036010.
[78] J. Huber, N. Fleck, M. Ashby, *Proc. R. Soc. London, Ser. A* **1997**, *453*, 2185.
[79] H. F. Ali, Y. Kim, presented at *Information Storage and Processing Systems*, Virtual, June, **2021**.
[80] A. Riccio, C. Napolitano, A. Sellitto, V. Acanfora, M. Zarrelli, *Sensors* **2021**, *21*, 5506.
[81] M. Sansone, S. Ameduri, A. Concilio, E. Cestino, *Actuators* **2022**, *11*, 81.
[82] S.-H. Ahn, K.-T. Lee, H.-J. Kim, R. Wu, J.-S. Kim, S.-H. Song, *Int. J. Precis. Eng. Manuf.* **2012**, *13*, 631.
[83] R. Dauksher, Z. Patterson, C. Majidi, *Actuators* **2021**, *10*, 202.
[84] W. Wang, Y. Tang, C. Li, *Int. J. Mech. Sci.* **2021**, *193*, 106181.
[85] H.-J. Kim, S.-H. Song, S.-H. Ahn, *Smart Mater. Struct.* **2012**, *22*, 014007.
[86] L. P. Kollar, G. S. Springer, *Mechanics of Composite Structures*, Cambridge University Press, Cambridge **2003**.
[87] S.-H. Song, H. Lee, J.-G. Lee, J.-Y. Lee, M. Cho, S.-H. Ahn, *Composites, Part B* **2016**, *95*, 155.
[88] H. Rodrigue, B. Bhandari, M.-W. Han, S.-H. Ahn, *J. Intell. Mater. Syst. Struct.* **2015**, *26*, 1071.
[89] H. Rodrigue, W. Wang, B. Bhandari, M.-W. Han, S.-H. Ahn, *Composites, Part B* **2015**, *82*, 152.
[90] M.-W. Han, H. Rodrigue, S. Cho, S.-H. Song, W. Wang, W.-S. Chu, S.-H. Ahn, *Composites, Part B* **2016**, *86*, 285.
[91] M.-W. Han, H. Rodrigue, H.-I. Kim, S.-H. Song, S.-H. Ahn, *Compos. Struct.* **2016**, *140*, 202.
[92] M. W. Han, S. H. Ahn, *Adv. Mater.* **2017**, *29*, 1606580.
[93] N. K. Persson, J. G. Martinez, Y. Zhong, A. Maziz, E. W. Jager, *Adv. Mater. Technol.* **2018**, *3*, 1700397.
[94] V. Sanchez, C. J. Walsh, R. J. Wood, *Adv. Funct. Mater.* **2021**, *31*, 2008278.
[95] A. A. M. Faudzi, M. R. M. Razif, I. N. A. M. Nordin, K. Suzumori, S. Wakimoto, D. Hirooka, presented at *2012 IEEE/ASME Int. Conf. Advanced Intelligent Mechatronics (AIM)*, Taiwan, July, **2012**.
[96] J. San Juan, M. L. Nó, C. A. Schuh, *Adv. Mater.* **2008**, *20*, 272.
[97] Y. Q. Fu, S. Zhang, M. Wu, W. M. Huang, H. Du, J. Luo, A. Flewitt, W. Milne, *Thin Solid Films* **2006**, *515*, 80.
[98] A. Ibarra, D. Caillard, J. San Juan, M. Nó, *Appl. Phys. Lett.* **2007**, *90*, 101907.
[99] M. Reinhold, D. Kiener, W. B. Knowlton, G. Dehm, P. Müllner, *J. Appl. Phys.* **2009**, *106*, 053906.
[100] J. Peirs, D. Reynaerts, H. Van Brussel, presented at *Proc. 1998 IEEE Int. Conf. Robotics Automation (Cat. No. 98CH36146)*, Belgium, May, **1998**.
[101] A. AbuZaiter, M. Nafea, M. S. M. Ali, *Mechatronics* **2016**, *38*, 16.
[102] Z. Wang, G. Hang, Y. Wang, J. Li, W. Du, *Smart Mater. Struct.* **2008**, *17*, 025039.
[103] P. Karna, S. M. Prabu, S. Karthikeyan, R. Mithun, S. Jayachandran, N. Resnina, S. Belyaev, I. Palani, *Sens. Actuators, A* **2021**, *321*, 112411.
[104] S. Takeuchi, I. Shimoyama, *J. Microelectromech. Syst.* **2000**, *9*, 24.
[105] J. J. Gill, K. Ho, G. P. Carman, *J. Microelectromech. Syst.* **2002**, *11*, 68.
[106] H. J. Lee, J. J. Lee, *Smart Mater. Struct.* **2000**, *9*, 817.
[107] M. S. M. Ali, B. Bycraft, A. Bsoul, K. Takahata, *J. Microelectromech. Syst.* **2012**, *22*, 331.
[108] K. H. Low, J. Yang, A. P. Pattathil, Y. Zhang, presented at *2006 IEEE Int. Conf. Automation Science Engineering*, China, October, **2006**.
[109] I. Roch, P. Bidaud, D. Collard, L. Buchaillot, *J. Micromech. Microeng.* **2003**, *13*, 330.
[110] W. L. Benard, H. Kahn, A. H. Heuer, M. A. Huff, *J. Microelectromech. Syst.* **1998**, *7*, 245.
[111] A. P. Jardine, J. S. Madsen, P. G. Mercado, *Mater. Charact.* **1994**, *32*, 169.
[112] P. Krulevitch, A. P. Lee, P. B. Ramsey, J. C. Trevino, J. Hamilton, M. A. Northrup, *J. Microelectromech. Syst.* **1996**, *5*, 270.
[113] C. Smith, A. Villanueva, K. Joshi, Y. Tadesse, S. Priya, *Smart Mater. Struct.* **2010**, *20*, 012001.
[114] J. H. Crews, J. A. McMahan, R. C. Smith, J. C. Hannen, *Smart Mater. Struct.* **2013**, *22*, 115021.
[115] Y. Du, B. Liu, M. Xu, E. Dong, S. Zhang, J. Yang, *Mechatronics* **2015**, *25*, 18.
[116] G. Zhou, P. Lloyd, *Compos. Sci. Technol.* **2009**, *69*, 2034.
[117] J.-S. Koh, *Materials* **2018**, *11*, 2324.
[118] W. Wang, C. Y. Yu, P. A. Abrego Serrano, S.-H. Ahn, *Soft Rob.* **2020**, *7*, 283.
[119] N.-G. Kim, M.-W. Han, A. Iakovleva, H.-B. Park, W.-S. Chu, S.-H. Ahn, *Compos. Struct.* **2020**, *243*, 112227.
[120] H.-B. Park, D.-R. Kim, H.-J. Kim, W. Wang, M.-W. Han, S.-H. Ahn, *Int. J. Precis. Eng. Manuf.* **2020**, *21*, 249.
[121] H.-S. Kim, J.-K. Heo, I.-G. Choi, S.-H. Ahn, W.-S. Chu, *Bioinspiration Biomimetics* **2021**, *16*, 066006.

[122] H. Rodrigue, W. Wang, D.-R. Kim, S.-H. Ahn, *Compos. Struct.* **2017**, *176*, 398.
[123] W. Wang, S.-H. Ahn, *Soft Rob.* **2017**, *4*, 379.
[124] M.-S. Kim, W.-S. Chu, J.-H. Lee, Y.-M. Kim, S.-H. Ahn, *Int. J. Precis. Eng. Manuf.* **2011**, *12*, 565.
[125] M. Kim, Y.-J. Shin, J.-Y. Lee, W.-S. Chu, S.-H. Ahn, *Int. J. Precis. Eng. Manuf.* **2017**, *18*, 895.
[126] H.-T. Lee, S.-I. Kim, J. M. Park, H.-J. Kim, D.-S. Song, H.-I. Kim, H.-G. Wu, S.-H. Ahn, *J. Comput. Des. Eng.* **2015**, *2*, 176.
[127] W. Wang, H. Rodrigue, S.-H. Ahn, *Composites, Part B* **2015**, *78*, 507.
[128] H. Rodrigue, W. Wang, B. Bhandari, M.-W. Han, S.-H. Ahn, *Int. J. Precis. Eng. Manuf.-Green Technol.* **2014**, *1*, 153.
[129] J.-S. Kim, J.-Y. Lee, K.-T. Lee, H.-S. Kim, S.-H. Ahn, *J. Mech. Sci. Technol.* **2013**, *27*, 3123.
[130] J. Ryu, B.-S. Jung, M.-S. Kim, J. Kong, M. Cho, S.-H. Ahn, *J. Intell. Mater. Syst. Struct.* **2011**, *22*, 1941.
[131] M. Han, X. Guo, X. Chen, C. Liang, H. Zhao, Q. Zhang, W. Bai, F. Zhang, H. Wei, C. Wu, *Sci. Rob.* **2022**, *7*, eabn0602.
[132] A. Thabuis, S. Thomas, T. Martinez, P. Germano, Y. Perriard, *Smart Mater. Struct.* **2021**, *30*, 095025.
[133] A. M. Hoover, E. Steltz, R. S. Fearing, presented at *2008 IEEE/RSJ Int. Conf. Intelligent Robots Systems*, France, September, **2008**.
[134] S. Seok, C. D. Onal, K.-J. Cho, R. J. Wood, D. Rus, S. Kim, *IEEE/ASME Trans. Mechatron.* **2012**, *18*, 1485.
[135] W. Wang, J.-Y. Lee, H. Rodrigue, S.-H. Song, W.-S. Chu, S.-H. Ahn, *Bioinspiration Biomimetics* **2014**, *9*, 046006.
[136] J.-S. Koh, K.-J. Cho, *IEEE/ASME Trans. Mechatron.* **2012**, *18*, 419.
[137] X. Huang, K. Kumar, M. K. Jawed, A. Mohammadi Nasab, Z. Ye, W. Shan, C. Majidi, *Adv. Mater. Technol.* **2019**, *4*, 1800540.
[138] R. M. Bena, X.-T. Nguyen, A. A. Calderón, A. Rigo, N. O. Pérez-Arancibia, *IEEE Rob. Autom. Lett.* **2021**, *6*, 8173.
[139] Z. Zhakypov, K. Mori, K. Hosoda, J. Paik, *Nature* **2019**, *571*, 381.
[140] J. Hwang, W. D. Wang, *Adv. Mater. Technol.* **2022**, *7*, 2101153.
[141] H.-S. Kim, J.-Y. Lee, W.-S. Chu, S.-H. Ahn, *Soft Rob.* **2017**, *4*, 49.
[142] A. Villanueva, C. Smith, S. Priya, *Bioinspiration Biomimetics* **2011**, *6*, 036004.
[143] M. Muralidharan, I. Palani, *Def. Sci. J.* **2021**, *71*, 94.
[144] M. D. Bartlett, N. Kazem, M. J. Powell-Palm, X. Huang, W. Sun, J. A. Malen, C. Majidi, *Proc. Natl. Acad. Sci. USA* **2017**, *114*, 2143.
[145] J.-S. Koh, E. Yang, G.-P. Jung, S.-P. Jung, J. H. Son, S.-I. Lee, P. G. Jablonski, R. J. Wood, H.-Y. Kim, K.-J. Cho, *Science* **2015**, *349*, 517.
[146] M. Noh, S.-W. Kim, S. An, J.-S. Koh, K.-J. Cho, *IEEE Trans. Rob.* **2012**, *28*, 1007.
[147] Y. S. Chung, J.-H. Lee, J. H. Jang, H. R. Choi, H. Rodrigue, *ACS Appl. Mater. Interfaces* **2019**, *11*, 40793.
[148] J. Colorado, A. Barrientos, C. Rossi, K. S. Breuer, *Bioinspiration Biomimetics* **2012**, *7*, 036006.
[149] S. J. Furst, G. Bunget, S. Seelecke, *Smart Mater. Struct.* **2012**, *22*, 014011.
[150] J.-H. Lee, Y. S. Chung, H. Rodrigue, *Sci. Rep.* **2019**, *9*, 11251.
[151] H.-I. Kim, M.-W. Han, S.-H. Song, S.-H. Ahn, *Composites, Part B* **2016**, *105*, 138.
[152] J. Yin, T. Hellebrekers, C. Majidi, presented at *2020 3rd IEEE Int. Conf. Soft Robotics (RoboSoft)*, USA, May, **2020**.
[153] Z. J. Patterson, A. P. Sabelhaus, C. Majidi, *IEEE Rob. Autom. Lett.* **2022**, *7*, 2210.
[154] A. T. Haque, R. Tutika, R. L. Byrum, M. D. Bartlett, *Adv. Funct. Mater.* **2020**, *30*, 2000832.
[155] M. Kohl, B. Krevet, E. Just, *Sens. Actuators, A* **2002**, *97*, 646.
[156] H. T. Lee, F. Seichepine, G. Z. Yang, *Adv. Funct. Mater.* **2020**, *30*, 2002510.
[157] C. Gonçalves, A. F. da Silva, R. Simoes, J. Gomes, L. Stirling, B. Holschuh, *IEEE/ASME Trans. Mechatron.* **2019**, *24*, 1464.
[158] R. Granberry, J. Barry, B. Holschuh, J. Abel, *Adv. Mater. Technol.* **2021**, *6*, 2000825.
[159] S. J. Park, C. H. Park, *Sci. Rep.* **2019**, *9*, 9157.
[160] C. Kim, G. Kim, Y. Lee, G. Lee, S. Han, D. Kang, S. H. Koo, J.-s. Koh, *Smart Mater. Struct.* **2020**, *29*, 055003.
[161] J. Jeong, I. B. Yasir, J. Han, C. H. Park, S.-K. Bok, K.-U. Kyung, *Appl. Sci.* **2019**, *9*, 4025.
[162] S.-M. Lee, W.-K. Jung, J. Park, S.-H. Ahn, *Fashion Text.* **2022**, *9*, 11.
[163] D. Kim, B. Kim, B. Shin, D. Shin, C.-K. Lee, J.-S. Chung, J. Seo, Y.-T. Kim, G. Sung, W. Seo, S. Kim, S. Hong, S. Hwang, S. Han, D. Kang, H.-S. Lee, J.-S. Koh, *Nat. Commun.* **2022**, *13*, 4155.
[164] G. Costanza, M. E. Tata, *Materials* **2020**, *13*, 1856.
[165] J. K. Strelec, D. C. Lagoudas, M. A. Khan, J. Yen, *J. Intell. Mater. Syst. Struct.* **2003**, *14*, 257.
[166] NASA, National Aeronautics and Space Administration, https://technology.nasa.gov/patent/LEW-TOPS-99 (accessed: May **2022**).
[167] J. H. Crews, G. D. Buckner, *J. Intell. Mater. Syst. Struct.* **2012**, *23*, 545.
[168] A. T. Tung, B.-H. Park, D. H. Liang, G. Niemeyer, *Sens. Actuators, A* **2008**, *147*, 83.
[169] J. Sheng, X. Wang, T.-M. L. Dickfeld, J. P. Desai, *IEEE Rob. Autom. Lett.* **2018**, *3*, 4038.
[170] M. Boyvat, J.-S. Koh, R. J. Wood, *Sci. Rob.* **2017**, *2*, eaan1544.
[171] J. B. Gafford, R. J. Wood, C. J. Walsh, presented at *2017 IEEE Int. Conf. Robotics Automation (ICRA)*, Singapore, May, **2017**.
[172] A. Yamada, Y. Shiraishi, T. Sugai, H. Miura, T. Shiga, M. Hashem, C. Koga, H. Hashimoto, Y. Tsuboko, T. Yambe, presented at *World Congress Medical Physics Biomedical Engineering*, Beijing, China, May **2013**.
[173] K. Aarnink, F. Halfwerk, S. A. Saïd, J. Grandjean, J. Paulusse, *Cardiovasc. Eng. Technol.* **2019**, *10*, 1.
[174] N. A. Mansour, T. Jang, H. Baek, B. Shin, B. Ryu, Y. Kim, *Sens. Actuators, A* **2020**, *310*, 112024.
[175] D. Kim, I. Ferretto, C. Leinenbach, W. Lee, *Adv. Mater. Interfaces* **2022**, *9*, 2200171.
[176] A. N. Alagha, S. Hussain, W. Zaki, *Mater. Des.* **2021**, *204*, 109654.
[177] M. P. Caputo, A. E. Berkowitz, A. Armstrong, P. Müllner, C. V. Solomon, *Addit. Manuf.* **2018**, *21*, 579.
[178] L. Xue, K. Atli, S. Picak, C. Zhang, B. Zhang, A. Elwany, R. Arroyave, I. Karaman, *Acta Mater.* **2021**, *215*, 117017.
[179] J. Ma, B. Franco, G. Tapia, K. Karayagiz, L. Johnson, J. Liu, R. Arroyave, I. Karaman, A. Elwany, *Sci. Rep.* **2017**, *7*, 46707.
[180] A. Y. Lee, J. An, C. K. Chua, *Engineering* **2017**, *3*, 663.
[181] B. Holschuh, E. Obropta, D. Newman, presented at *2013 NASA Human Research Program (HRP) Investigators' Workshop*, USA, February, **2013**.
[182] B. T. Holschuh, *Ph.D. Thesis*, Massachusetts Institute of Technology **2014**.
[183] Q. Liu, W. Wang, M. F. Reynolds, M. C. Cao, M. Z. Miskin, T. A. Arias, D. A. Muller, P. L. McEuen, I. Cohen, *Sci. Rob.* **2021**, *6*, eabe6663.
[184] D. Kim, M. Kim, S. Reidt, H. Han, A. Baghizadeh, P. Zeng, H. Choi, J. Puigmartí-Luis, M. Trassin, B. J. Nelson, *Nat. Commun.* **2023**, *14*, 750.
[185] J. Cui, T.-Y. Huang, Z. Luo, P. Testa, H. Gu, X.-Z. Chen, B. J. Nelson, L. J. Heyderman, *Nature* **2019**, *575*, 164.
[186] Y. S. Zhang, A. Khademhosseini, *Science* **2017**, *356*, eaaf3627.
[187] D. Han, C. Farino, C. Yang, T. Scott, D. Browe, W. Choi, J. W. Freeman, H. Lee, *ACS Appl. Mater. Interfaces* **2018**, *10*, 17512.
[188] R. D. Harris, J. T. Auletta, S. A. M. Motlagh, M. J. Lawless, N. M. Perri, S. Saxena, L. M. Weiland, D. H. Waldeck, W. W. Clark, T. Y. Meyer, *ACS Macro Lett.* **2013**, *2*, 1095.
[189] H. Yuk, S. Lin, C. Ma, M. Takaffoli, N. X. Fang, X. Zhao, *Nat. Commun.* **2017**, *8*, 14230.
[190] A. du Plessis d'Argentré, S. Perry, Y. Iwata, H. Iwasaki, E. Iwase, A. Fabozzo, I. Will, D. Rus, D. D. Damian, S. Miyashita, presented

at *2018 IEEE Int. Conf. Robotics Automation (ICRA)*, Australia, May, **2018**.
[191] H.-W. Huang, M. S. Sakar, A. J. Petruska, S. Pané, B. J. Nelson, *Nat. Commun.* **2016**, *7*, 12263.
[192] O. Erol, A. Pantula, W. Liu, D. H. Gracias, *Adv. Mater. Technol.* **2019**, *4*, 1900043.
[193] J. C. Breger, C. Yoon, R. Xiao, H. R. Kwag, M. O. Wang, J. P. Fisher, T. D. Nguyen, D. H. Gracias, *ACS Appl. Mater. Interfaces* **2015**, *7*, 3398.
[194] J.-C. Kuo, H.-W. Huang, S.-W. Tung, Y.-J. Yang, *Sens. Actuators, A* **2014**, *211*, 121.
[195] A. Ghosh, L. Li, L. Xu, R. P. Dash, N. Gupta, J. Lam, Q. Jin, V. Akshintala, G. Pahapale, W. Liu, *Sci. Adv.* **2020**, *6*, eabb4133.
[196] S. Pandey, E. Gultepe, D. H. Gracias, *J. Visualized Exp.* **2013**, *72*, e50022.
[197] H. Lee, C. Xia, N. X. Fang, *Soft Matter* **2010**, *6*, 4342.
[198] S.–M. An, J. Ryu, M. Cho, K.-J. Cho, *Smart Materials and Structures* **2012**, *21*, 055009.
[199] R. Granberry, K. Eschen, B. Holschuh, J. Abel, *Advanced Materials Technologies* **2019**, *4*, 1900548.
[200] S. M. Mirvakili, I. W. Hunter, *ACS Applied Materials & Interfaces* **2017**, *9*, 16321.
[201] S. M. Mirvakili, I. W. Hunter, Electroactive Polymer Actuators and Devices (EAPAD) 2017, **2017**, https://doi.org/10.1117/12.2261712

Min-Soo Kim is a postdoctoral associate at the Institute of Robotics and Intelligent Systems, ETH Zürich. He received his Ph.D. in 2018 for mechanical engineering from the Seoul National University. His research interests include functional/composite materials, small-scale robotics, sensors/actuators, and micro-/nanotechnology.

Salvador Pané is a professor of materials for robotics and co-director of the Multi-Scale Robotics Lab (MSRL) at the ETH Zürich. He received his Ph.D. in chemistry from the University of Barcelona in 2008 and subsequently joined MSRL as a postdoctoral researcher in August 2008. He has been awarded the highly competitive ERC-StG and ERC-CoG in 2012 and 2017, respectively. His interests lie in bridging materials science, chemistry, and electrochemistry with small-scale robotics for various applications.

Min-Woo Han is an assistant professor in the Department of Mechanical, Robotics, and Energy Engineering at the Dongguk University. He received his Ph.D. in mechanical engineering at the Seoul National University in 2017. He continued his research as a postdoctoral fellow at the Harvard University, 2017–2018. His research interests include soft actuators/sensors, smart materials, 3D/4D printing, and advanced manufacturing technologies.

Sung-Hoon Ahn is currently a professor and the chair of the Department of Mechanical Engineering, Seoul National University. He received his Ph.D. in 1997 for aeronautics and astronautics from the Stanford University. He is serving as an outside director under Hyundai WIA Corp, president of the Academic Society for Appropriate Technology, and vice president of the Korean Society of Precision Engineering. His research interests include smart factories, smart grids, appropriate technology, sensors/actuators, robotics, smart/composite materials, micro-/nanotechnology, 3D/4D printing, and green manufacturing. He has published over 360 peer-reviewed journal articles, over 70 granted patents, and supervised over 110 graduate students.